Identifying the Cretaceous–Paleogene boundary in North Dakota, USA, using portable XRF

Emilie Larsson

Dissertations in Geology at Lund University,
Bachelor's thesis, no. 356
(15 hp/ECTS credits)

Department of Geology
Lund University
2013

Identifying the Cretaceous–Paleogene boundary in North Dakota, USA, using portable XRF

Bachelor's thesis

Emilie Larsson

Department of Geology
Lund University
2013

Contents

Cover Picture: Field photo from Mud Buttes section (modified from Antoine Bercovici 2011).

Identifying the Cretaceous–Paleogene boundary in North Dakota, USA, using portable XRF

EMILIE LARSSON

Larsson, E., 2013: Identifying the Cretaceous–Paleogene boundary in North Dakota, USA, using portable XRF. *Dissertations in Geology at Lund University*, No. 356, 34 pp. 15 hp (15 ECTS credits).

Abstract: A portable x-ray fluorescence (XRF) device was in this study used to identify geochemical markers associated with the Cretaceous–Paleogene boundary in North Dakota, USA. At the time of the K–Pg boundary, an asteroid struck the Earth which resulted in one of the five big mass extinctions. The event left behind a globally distributed clay layer consisting of material derived from the asteroid and the impact site. The two analyzed sections consists of terrestrial deposits with the K-Pg boundary layer preserved. The portable XRF device analyses the chemical composition by exposing the samples to x-rays and detect the fluorescence x-rays emitted by exciting electrons. Results obtained in this study show that many elements are elevated in the boundary clay layer at both studied sections. Of these, several elements can be linked to the K–Pg event thus they are found as compounds in meteorites or are common constituents in the platform carbonates found in the area of impact in Yucatán. A total of 19 elements display prominent peaks at the boundary and of these Cr, Ni and Ti most certainly derived from the impactor while As, S, Ca and U likely derived from the platform carbonates at the impact site. The results display a good correlation to geochemical trends at other studied K–Pg sections in the world and demonstrate that a portable XRF is a useful tool for detection of the K–Pg boundary with applications in the lab as well as in the field.

Keywords: Portable XRF, K–Pg boundary, geochemistry, terrestrial deposits, North Dakota.

Supervisor: Antoine Bercovici

Subject: Bedrock Geology

Emilie Larsson, Department of Geology, Lund University, Sölvegatan 12, SE-223 62 Lund, Sweden.
E-mail: emilierlarsson@hotmail.com

Identifiering av Krita–Paleogengränsen i North Dakota, USA, med portabel XRF

EMILIE LARSSON

Larsson, E., 2013: Identifiering av Krita–Paleogengränsen i North Dakota, USA, med portabel XRF. *Examensarbeten i geologi vid Lunds universitet*, Nr. 356, 34 sid. 15 hp.

Sammanfattning: En portabel röntgenfluorescens (XRF) spektrometer användes i denna studie för att identifiera kemiska markörer relaterade till Krita–Paleogen (K–Pg) gränsen i North Dakota, USA. Vid K–Pg-gränsen träffades jorden av en asteroid vilket resulterade i ett av de fem stora massutdöendena. Nedslaget lämnade efter sig ett globalt spritt lerlager bestående av material från asteroiden samt berggrund från karbonatplattformen i dagens Yucatán, Mexico, som utgjorde nedslagsplatsen. De två analyserade sektionerna i denna studie består av terrestra avlagringar och har K–Pg lerlagret bevarat. Ett flertal grundämnen uppvisar förhöjda värden i detta lager och av dessa kan flertalet kopplas samman med K–Pg gränsen då de är beståndsdelar i meteoriter eller vanliga i berggrunden som utgör nedslagsplatsen. Totalt 19 grundämnen uppvisar förhöjda värden vid gränslagret, av dessa härstammar Cr, Ni och Ti sannolikt från meteoriten medan As, S, Ca och U sannolikt har sitt ursprung i plattformskarbonaterna vid nedslagsplatsen. Jämförande studier av geokemiska trender vid andra K–Pg lagergränser i världen uppvisar i många fall god korrelation. Detta visar att portabel XRF analys är ett bra hjälpmedel för att detektera K–Pg gränsen, användbar vid både laboratorie- och fältarbete.

Nyckelord: Portabel XRF, K–Pg gränsen, geokemi, terrestra avlagringar, North Dakota.

Emilie Larsson, Geologiska institutionen, Lunds universitet, Sölvegatan 12, 223 62 Lund, Sverige.
E-post: emilierlarsson@hotmail.com

1. Introduction

66 million years ago an asteroid with a diameter of approximately 10 km struck the earth in the Yucatán peninsula (Alvarez et al. 1980; Hildebrand et al. 1991; Renne et al. 2013). The high energy impact generated a global spread of material into the atmosphere which shut out the sunlight preventing photosynthesis (Vajda et al. 2001). Additionally the event created instant atmospheric heating, acid rains, lower temperatures, thinner ozone, enhanced erosion and greenhouse warming (Kring 2007). These effects triggered one of the five largest mass extinctions known today; affecting both terrestrial and marine life forms (Alvarez et al. 1980).

The centre of the impact is located under the village Chicxulub, Mexico, forming a 200 km wide crater in platform carbonates overlying a crystalline basement (Hildebrand et al. 1991).

The material ejected at the impact formed the K–Pg boundary impact layer which occurs in the stratigraphic record all around the world and forms the boundary between the Cretaceous and the Paleogene (Alvarez et al. 1980). The layer typically contains spherules, shocked quartz and abnormally high concentrations of platinum group elements. Among the platinum group elements Ir is the most important as it originates from the asteroid itself and is depleted in Earths crust (Alvarez et al. 1980). The impact layer can consist of up to three ballistically ejected layers increasing in thickness with decreased distance from the Chicxulub crater (Sweet et al. 1999; Schulte et al. 2010). The basal layer, here referred to as the K–Pg boundary claystone (Izett 1990) represents the low angle ejecta formed by melted rock from the impact area (Sweet et al. 1999).This is followed by the spherule layer representing the high angle ejecta (Izett 1990) formed by condensed material from the fireball created at the impact (Sweet et al. 1999).The upper layer, here referred to as the Ir-anomaly layer, represents the distal ejecta layer with the finest fractions containing shocked quarts and the highest Ir-anomaly values (Lerbekmo 1999).

The K–Pg boundary has been recovered in both terrestrial and marine sediments. These separate depositional environments may give rise to boundary clays with different characteristics due to the disparity in the physical and chemical environments.

The known age of the K–Pg boundary and its coevality all over the globe makes it a global marker bed, helpful in dating sediments. Identification of the boundary can be made with lithological and mineralogical markers in form of spherules and shocked quarts formed by material from the blast and airfall. Additionally, biostratigraphy can be used as the asteroid triggered the extinction with disappearance of numerous animals and plants, both on land and in the sea. Thus the recognition of species disappearance and loss of diversity can be used. In some areas the K–Pg boundary does not show characteristic trends or visible boundary clay layer. In these areas geochemical markers can be the only way to identify the boundary and separate the Cretaceous from the Paleogene in the field making a portable instrument for element analysis crucial.

A handheld X-ray fluorescence (XRF) device was here for the first time used to analyse the geochemistry of two K–Pg boundary sections in North Dakota. XRF is a tool for elemental analysis that has undergone great development over the last 10 years, going from room sized equipment to small portable devices (Fig. 1a and 1b). The aim of this study will be to evaluate the usefulness of portable XRF analysis in identifying element anomalies that could be associated with the K–Pg boundary.

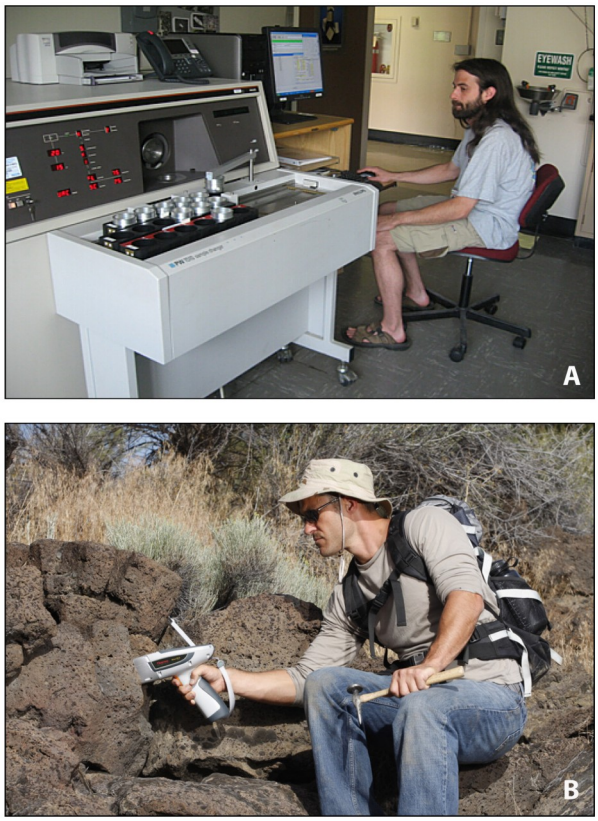

Fig. 1. **a.** Stationary XRF device, taking up an entire room. Modified after Smithsonian National museum of Natural History (2013; http://mineralsciences.si.edu/facilities/xrf.htm). **b**. Portable XRF device. Modified after Thermo Fisher Scientific (2013; http://www.portableas.com/index.php/products/niton-xl3t-950-goldd/).

2. Geological setting

This study is based on samples that were collected from two sections located in the southwestern part of North Dakota, USA. The outcrops are situated parallel to the Cedar Creek anticline in the badlands along the Little Missouri River. The lower part of the sections is located in the Hell Creek Formation which is of late Maastrichian age and the upper part is located in the Fort Union Formation of early Paleocene age (Johnson et al 2002; Bercovici 2009). Both sections consist of

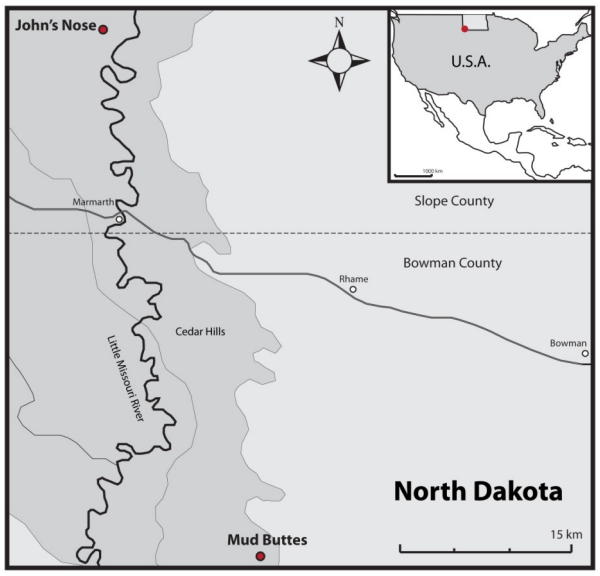

Fig. 2. Map of the United States and the southwest corner of North Dakota where the sections John's Nose and Mud Buttes are situated. John's Nose is located in the northwest corner on the map with coordinates (lat., long.) 46.4401496, -103.939020 and Mud buttes in the maps southern part with coordinates (lat., long.) 46.019853, -103.762779.

terrestrial deposits with the K–Pg boundary clay layer preserved. A map over the area can be seen in Fig. 2.

2.1 John's Nose section

The northernmost locality John's Nose is situated in Slope County (Fig. 2). The vertical extent of the section is approximately 1.8 meters and the lithology that will be described hereinafter (Fig. 3). The base of the section consists of 16 cm of muddy siltstone (unit 1 and 2) which is part of the Hell Creek Formation. This is followed by a 20 cm thick coal layer (unit 3) representing the beginning of the Fort Union Formation. The coal is overlain by 28 cm silty mudstone (unit 4) which is followed by a 3 cm thick clay layer (unit 5 and 6). This layer is usually referred to as the boundary clay layer separating the Cretaceous from the Paleogene (Bercovici et al. 2012). At this section the layer is divided in to two parts, the boundary claystone layer and the spherule layer. A 4.5 cm coal layer (unit 7) is overlaying the boundary clay followed by 61 cm of silty mudstone (unit 8 and 9), 30 cm mudstone (unit 10) and an unmeasured unit of silty sandstone (unit 11).

2.1 Mud Buttes section

The southern locality Mud Buttes is located in Bowman County (Fig. 2). The stratigraphic interval from the K–Pg boundary in this section is the most complete in the area with physical, sedimentological and geo-

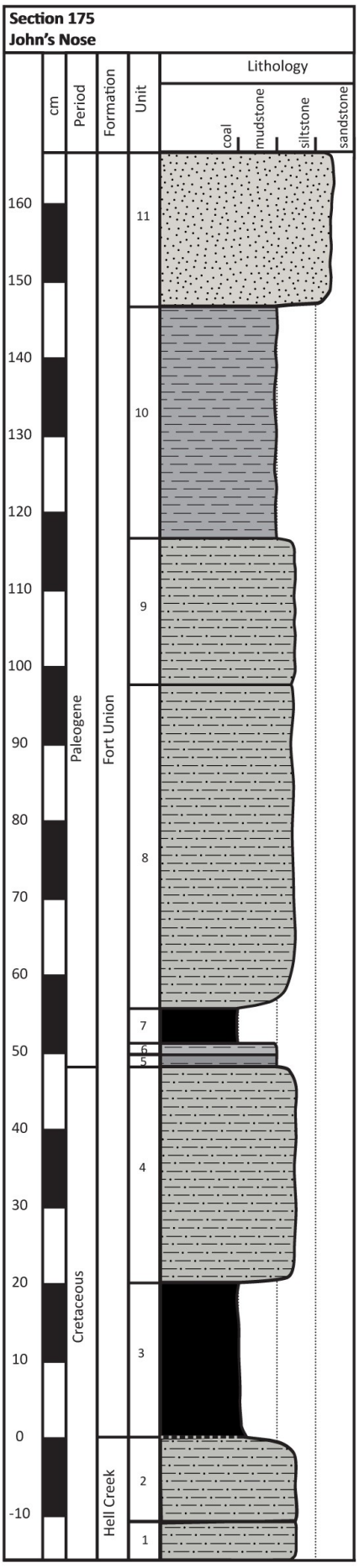

Fig. 3. Log of John's Nose section. The K–Pg boundary layer is in this section divided into two layers, the boundary clay layer succeeded by the spherule layer. These layers can be observed in unit 5 and 6.

Fig. 4. The boundary clay layer and the formation contact at John's Nose section seen in the field (from Bercovici 2011).

chemical evidence including spherules, shocked quarts and an Ir-anomaly. Here, the boundary clay coincides with the formation contact (Bercovici 2012). The examined part of the section is approximately 0.5 meters thick and is described below (Fig. 5).

The base the section consists of an unmeasured layer consisting of organic rich mudstone with gypsum (unit 1). This is overlain by the boundary clay layer consisting of three parts (unit 2, 3 and 4), the boundary clay layer (1.5 cm), the spherule layer (1 cm) and the Ir-anomaly layer (1.5 cm) which is organic rich containing charcoal. This is followed by a 41 cm thick silty mudstone layer (unit 5) with burrows, silt inclusions and a charcoal horizon in the lower part.

3. Method

A total of 66 samples from two sections were collected by Bercovici in 2011. 44 samples from the northern section John's Nose and 22 samples from the southern, Mud Buttes from which only 14 have been available. The samples were transported to Lund University in Sweden for XRF-analysis.

X-ray fluorescence is a widely used non-destructive elemental analysis with broad applications requiring minimum sample preparation. The method is based on the characteristic x-ray fluorescence spectrum of each element. The device exposes a sample to x-rays generated from an x-ray tube which excite electrons from atoms within the sample. The atoms then release the excitation energy back in form of x-rays (Fig. 6). The energy from the x-rays is then detected by a silicon detector and interpreted by a computer showing the concentration of each element (Arai 2006;

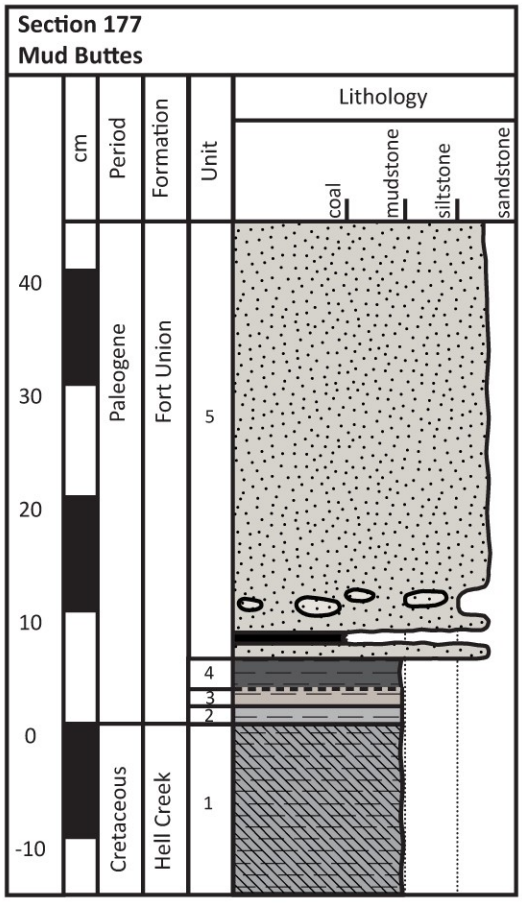

Fig. 5. Log of Mud Buttes section. In this section the K–Pg boundary is divided into three layers, the boundary clay layer, the spherule layer and the layer with the Ir-anomaly on the top. These layers can be observed in unit 2, 3 and 4.

Brouwer 2010).

Measurements of heavier elements are usually more accurate than those of lighter elements. This due to the fact that the lighter elements response closer to zero in the x-ray spectrum where more noise is present which lowers the measurement accuracy. Additionally, the measurement accuracy (precision) is related to the sample composition and the standard deviation. The ability to detect the elements depends on the element abundance, the sample precision and the XRF device.

Prior to analysis, the samples were crushed with an agate mortar making them more heterogeneous, potentially having positive result on the measurement accuracy. This was preformed in stratigraphic order to minimize negative effect of any contamination.

The XRF analysis of major trace elements was performed using a Niton XL3t Goldd+ XRF device at the Geological department at Lund University. The samples were placed on polypropylene X-ray film (TF-240) and analyzed on an 8mm area for 180 seconds in total. For enhanced measurement accuracy the samples were analysed in stratigraphic order and each sample was tested four times enabling average value calculations for improved accuracy.

For calibration and detection of drift standard sam-

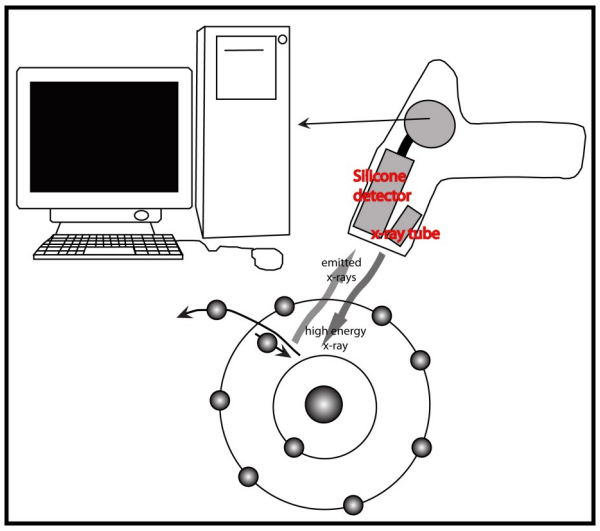

Fig. 6. Illustration of a portable XRF instrument and its basic physics.

ple 2709a with a known reference value was analysed every tenth sample. The difference between the reference value and the measured calibration value is a tool to evaluate the accuracy of the measurements. By comparing the percentage difference between the calibration samples with the known reference value potential drift can be detected.

4. Results

45 elements were measured during the XRF analysis in samples from Mud Buttes and John's Nose sections. Up to 19 elements display elevated values at or just above the K–Pg boundary, these values can be seen as plots in appendix Fig. 1 to 4. For all measured values see appendix Table 1 and 2. Elements completely below the detection limit and elements displaying no meaningful trends will not be discussed in the coming sections. The elements completely below the detection limit are Co, Ag, Cd, Sn, Sb, Au, Bi, Pd, Te, Cs, La, Ce, Pr and Nd. In measurements where the element concentration is below the detection limit (indicated by <LOD in appendix Table 1, 2 and 3) the value ranges between zero and the measured error value.

The calibration sample analysis shows a difference of 1–1000% between the measured value and the reference value with no major drift in the measurements. Most elements show a difference below 50% from the known standard. The largest difference from the standard value is shown by U (124%), Cu (142%), As (198%), P (240%), Sc (502%) and Cs (980%). Plot of the calibration values displaying the percentage deviation from the standard reference is shown in appendix Fig. 5, for numeric values see appendix Table 3.

4.1 John's Nose section

Several of the investigated elements show distinctive peaks at the K–Pg boundary in John's Nose section, more specifically Al, S, Ca, Ti, V, Cr, Cu, As, Se, Sr, Y, Nb, Mo, Pb, Th and U. These peak values are presented in Table 1. Additionally, all measured values are presented in appendix Table 1.

The elements with most prominent peaks at the K–Pg boundary is Ti, As, Al, Cr, Se, Pb and Nb. Ti display an instant increase in the spherule layer followed by a tailing effect upwards in the section. The highest value is approximately 11 times above that of the average above and below the boundary. Like Ti, As has high values in the spherule layer with values up to 7 times above average. Unlike the elements mentioned above, Se is frequently under the detection limit (<LOD) with 28 detected values displaying a significant peak in the spherule layer. Cr is like Se partly below the detection limit with only 8 values registered. The values reveal two peaks associated to the K–Pg boundary, one in the boundary clay and one at the base of the overlying coal layer.

Several elements have more prominent peaks in other layers but still display an elevation at the K–Pg boundary. Among these elements are U, V, S, Ca, Th and Mo. Both U and S is elevated in the spherule layer, but an even larger peak is seen in the succeeding coal layer. The Ca concentration is elevated in three parts of the section. The largest one in the last meter and a smaller in the boundary clay layer that display values approximately 5 times higher than in the surrounding samples.

A few elements show an elevated concentration not at the boundary but in the coal layer immediately above. Ni is partly under the detection limit and was recorded in 15 samples from which a few was detected just above the K–Pg boundary together with Cu.

Contrasting, some elements seemingly respond with a decline at the K–Pg boundary. These elements are the alkali metals K and Rb which behave in a similar fashion throughout the section. Zr, Y and Zn are responding in a similar manner with an instant increase in the overlaying coal layer. Common for these elements are that even though they show an overall decrease in the boundary they all seem to have a small peak in sample 175FU18 in the spherule layer. A single elevation in this sample is also seen in S and Ca. Al on the other hand displays a decline in the same sample.

The elements Rb, Ca, Si and K all increase in the upper meter of the section and Si values is at a low in the coal layers of the section, almost giving it a negative correlation to S.

Elements elevated at the boundary that will be discussed in the coming sections is displayed in Fig. 8. Additional plots of all elements elevated at the boundary can be seen in appendix Fig.1 and 2.

4.2 Mud Buttes section

In Mud Buttes Al, S, Ca, Sc, Ti, V, Cr, Fe, Ni, Cu, As, Se, Sr, Y, Zr, Mo, Pb, Th and U reveal distinctive peaks at the K–Pg boundary. The peak values at the boundary of these elements are presented in Table 1. Additionally, all measured values are presented in appendix Table 2.

Table 1. Peak values at or just above the K–Pg boundary at John's Nose and Mud Buttes measured with portable XRF. Samples are summed to one decimal and pared with the measured sample. All values given in ppm.

Element (ppm)	Mud Buttes	2σ	Sample	John's Nose	2σ	Sample
Al	80443.7	± 1805.9	177FU2	148066.3	± 3110.9	175FU19
S	26407.8	± 221	177FU4	17014.7	± 178.9	175FU18
Ca	16257.8	± 288.9	177FU4	7137.0	± 105.6	175FU18
Sc	105.1	± 29.8	177FU4			
Ti	11200.9	± 127.2	177FU2	42594.5	± 254.5	175FU19
V	463.8	± 31.7	177FU4	282	± 39.5	175FU19
Cr	275.7	± 26.1	177FU3	291.1	± 27.3	175FU22
Fe	62253.3	± 334.0	177FU2			
Ni	129.5	± 18.3	177FU4	295.3	± 24.2	175FU25
Cu	172	±10.7	177FU3	141.1	± 11.6	175FU25
As	301.7	± 10.4	177FU2	333.8	± 12.5	175FU19
Se	5.5	± 1.4	177FU4	10.3	± 1.9	175FU19
Sr	231.6	± 3.1	177FU3	340.7	± 3.7	175FU24
Y	51.4	± 1.7	177FU4	50.7	± 1.6	175FU23
Zr	600.1	± 4.9	177FU5	365.8	± 4.5	175FU25
Nb				25.0	± 1.4	175FU19
Mo	27.1	± 1.6	177FU4	14.4	± 1.7	175FU19
Pb	35.0	± 3.5	177FU2	41.3	± 3.7	175FU19
Th	16.2	± 4.1	177FU3	27.9	± 3.8	175FU19
U	28.2	± 2.8	177FU4	15.8	± 2.5	175FU19

Most measured elements display fluctuations near the K–Pg boundary layer, this usually in form of prominent peaks. Notably U and As which peak in the spherule layer exhibit values approximately 5 and 10 times greater than the average above and below the layer. The Ti and Pb values are raised during the entire K–Pg boundary sample sequence and like U and As they are high with values at least 2 times greater than the average. Cr, Ni and Se are all partly under the detection limit displaying respectively 7, 9 and 3 detected values. They all display a peak in the spherule layer at the top of the K–Pg boundary interval.

Distinct peaks outside of the K–Pg boundary interval is only seen in two elements. Ba which only displays two values above the detection limit shows a peak just above the K–Pg boundary interval. Like Ba, P displays elevated values at the base of the sediments succeeding the boundary interval with two distinctive peaks up to 10 times above average.

Several elements including Sr, Cu, S, Ca and U show similar trends including a stepwise increase in the spherule layer with a peak at the very top succeeded by a rapid decline. Unlike elements that shows an increase in the top of the spherule layer, Si show a decline in the same sample. The same pattern is shown by Al but unlike Si, Al also shows moderate elevation in the underlying spherule layer.

On the contrary, Si, Nb, Zn, Rb and K display a decrease in the K–Pg layers. Rb and K, both alkali metals follow the same trend with a decline in the boundary layer commenced by an increase in the overlaying silty mudstone. This rapid increase immediately above Ir-anomaly layer is also seen in Zn and Si.

The elevated elements discussed in the coming sections is plotted in Fig. 9. Additional plots can be seen in appendix Fig. 2 and 3.

5. Interpretations and discussion

The K–Pg boundary is in many cases detected geochemically by its high concentration of Ir. Ir and other platinum group elements may be of extraterrestrial origin and are one of the most used markers for the K–Pg event (Alvarez et al. 1980). Unfortunately elements like Ir occur in very low concentrations making them hard and time-consuming to identify (Gilmore et al. 1984). At Mud Buttes the Ir level was in a previous study measured to 1.38 ppb (Nichols and Johnson 2008). Portable XRF devices are merely able to measure values above 10 ppm, thus the Ir anomaly is 1000 times under its detection limit. The fact that the identification of one of the key elements is not always possible makes the identification of other elements related to the event crucial. Elements with easier and faster detection favour the future use of portable XRF for detection of the K–Pg boundary in field.

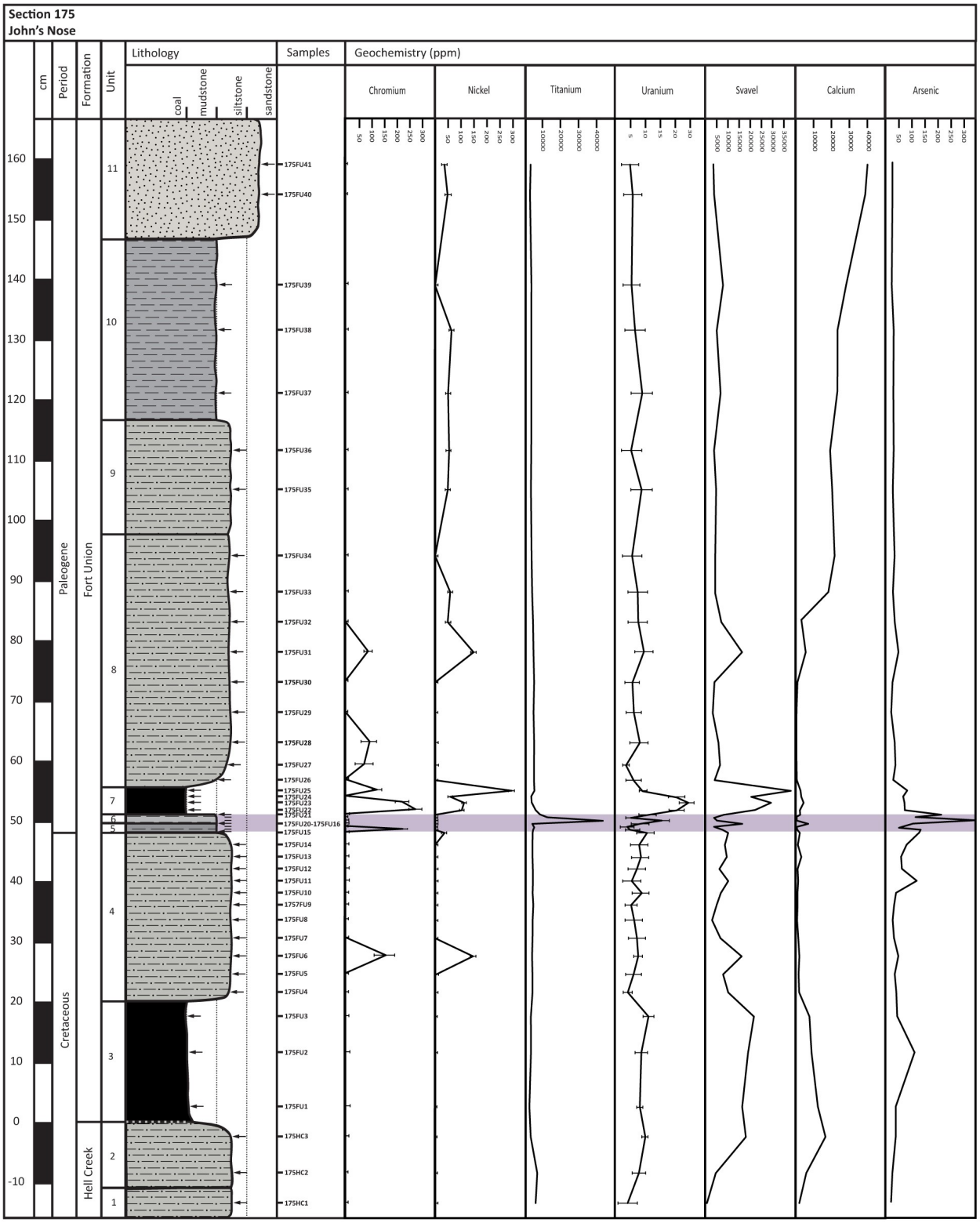

Fig. 8. Plot of the element concentrations in relation to the vertical section at John's Nose. Describes Cr, Ni, Ti, Ur, S, C and As values. The K–Pg boundary interval is marked by a purple area. Significant error is illustrated with error bars. Values in ppm.

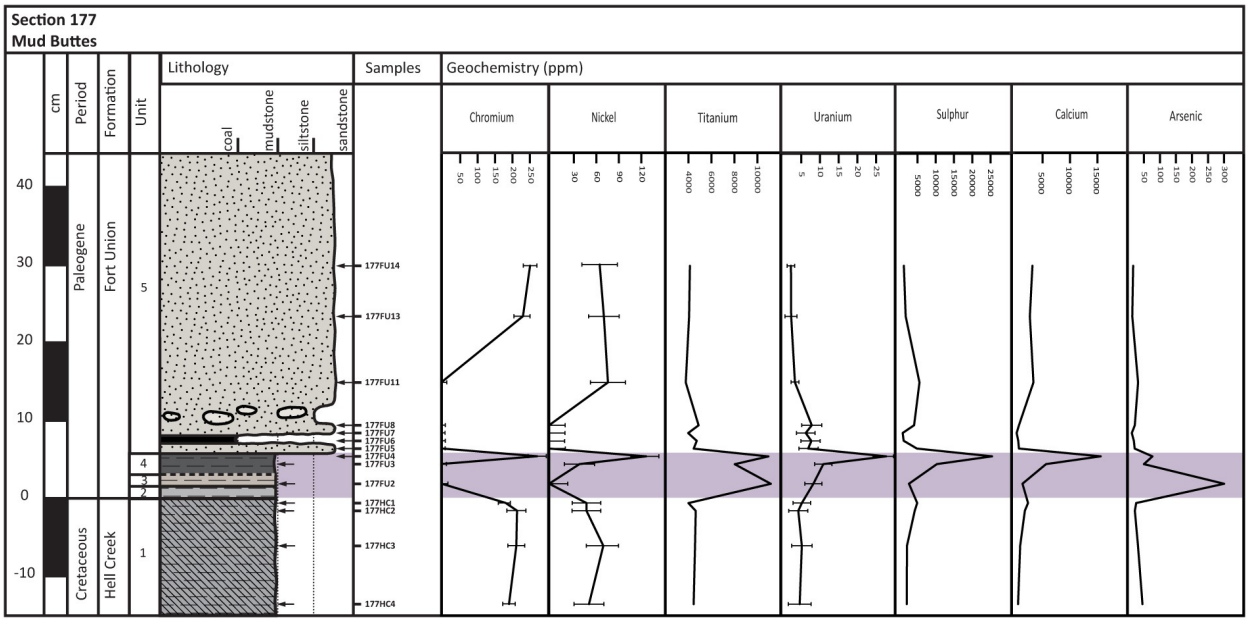

Fig. 9. Plot of the element concentrations at Mud Buttes in relation to the lithological section. Describes the Cr, Ni, Ti, U, S, Ca and As values at their correct positions in the section. K–Pg boundary is marked with a purple area. Significant error is illustrated as error bars and all values are given in ppm.

5.1 Comparison between John's Nose and Mud Buttes sections

A comparison of the John's Nose and Mud Buttes sections show that Al, S, Ca, Ti, V, Cr, Ni, Cu, As, Se, Y, Mo Pg, Th and U values are increased at the boundary samples at both locations. The elements commonly act correspondently in both sections though sometimes with slightly different concentrations (Fig. 8 and 9). Comparing the peak values in the two sections (Table 1) show that the difference between respective section ranges from 1–56 %. Differences between the two localities may derive from singularities in the depositional environment or the sampling process.

5.2 Geochemical variations linked to the K–Pg boundary

Elevated values at the K–Pg boundary have been detected in several elements. These elevations may or may not be linked to the K–Pg event. In the coming section some elevated elements likely linked to the event will be discussed.

Cr and Ni is often used to identify the K–Pg boundary and is shown to be elevated at both sections in this study. According to Barker & Anders (1968), Crocket & Kuo (1979) and Smit & ten Kate (1982) elevated values of Cr and Ni could originate from an extraterrestrial source that in this case would be the asteroid.

The Ti measurements display a prominent peak at the K–Pg boundary at both locations which according to Gilmore et al. (1984) and Izett (1990) are often seen and connected to the K–Pg boundary. Moore & Brown (1962) states that Ti together with Mn can be one of the more abundant elements in chondritic meteorites which is the type of impactor suggested by several authors (e.g. Alvarez et al. 1980; Smit & ten Kate 1982). In the standard K–Pg ejecta scenario the basal boundary clay layer mainly consists of material from the impact site while the succeeding fining upwards spherule layer also contain extraterrestrial material (Izett 1990).The Ti anomaly at John's Nose occurs in the spherule layer followed by a tailing off effect upwards. This indicates that the Ti anomaly seen in the K–Pg boundary at John's Nose could in fact have an extraterrestrial origin.

High concentrations of sulphur and calcium are present in the anhydrite ($CaSO_4$) rocks that make up almost one third of the impact area (Brett 1992; Ward et al. 1995; Wigforss-Lange et al. 2007). This could be the source of the elevated values of S and C seen in Mud Buttes and John's Nose K–Pg boundary layers. Additionally S has been obtained in meteorites (Hammond 2012) providing additional sources for the detected anomaly.

Furthermore, boundary clays have been found enriched in elements like As, Sb, U, Co and Zn (Wigforss-Lange et al. 2006). Some of these elements may originate from the impact area which is enriched in As, Sb, and U (Tuchscherer et al. 2005). Of these five elements, Sb and Co is under the detection limit and Zn is very fluctuating, not showing any major peak at the K–Pg boundary. Nonetheless, As and U values are showing prominent peaks at the boundary in both locations which may be linked to the K–Pg event and the impact area.

In a K–Pg boundary sample from Raton Basin, New Mexico, Gilmore et al. (1984) noticed elevated values of Sc, Ti, Cr, Hf and Ni. They also observed that the former three (Sc, Ti and Cr) have a strong pos-

itive correlation to Ir. Their interpretation is that these elevated values, together with V derive from post-impact fallout (Gilmore et al. 1984). These results correspond to the elevated values of Ti, Cr, Sc Ni and V seen at the two locations in the present study. Ti, Ni, Cr and V are known to occur in meteorites and other extraterrestrial objects (Smit & ten Kate 1982; Hammond 2012) implying that these elements may derive from the asteroid itself.

5.3 Geochemical variations linked to paleoenvironmental factors

Several elements including Rb, Ca, Si and K, common components in siliciclastic minerals, increase in the last meter of John's Nose and in the upper part of Mud Buttes section. Palynological data from John's Nose in a study by Bercovici et al. (2012) shows a decrease or disappearance of several plants in the sediments succeeding the K–Pg boundary. Additionally, a fern spike was detected indicating a decrease of terrestrial vegetation in this period (Bercovici et al. 2012). A decline in vegetation would make the ground unstable and more susceptible to erosional processes, explaining the sudden increased influx of silica minerals (Fig. 10).

5.4 Comparison with other published K–Pg boundary sites

Cr and Ni are two of the more important elements for identification of the K–Pg boundary (Smit & ten Kate 1982). In the performed study Cr is displaying elevated values at the K–Pg boundary at both localities. The peak at Mud buttes is 276 ±26 ppm at the top of the Ir-anomaly mudstone layer. At John's Nose the highest peak of 297 ±28 ppm is located in a sample at the base of the coal layer overlaying the K–Pg boundary layer. There is also a smaller peak at the base of the boundary clay in sample 175FU16 of 238 ±23 ppm. As a comparison, Cr levels measured in K–Pg boundary clay at Stevns Klint, Denmark, preformed with hard XRF show results of 371 ppm (Alvarez et al. 1980). Lower values are measured in Gubbio, Italy at 148.5 ppm (Smit & ten Kate 1982) and in Sugarite, USA (Gilmore et at. 1984) at 100 ppm using neutron activation analysis. Comparing the results from Stevns Klint, Gubbio and Sugarite localities, place John's Nose and Mud Buttes results between the values measured in Stevns Klint and Gubbio. The precision of the measurement is good with only 11-43 ppm error. A remark should be made on the calibration sampling of Cr showing values up to 80% above the known standard. This means that the measured values are plausibly higher than in reality. However, the inferred trend is correct.

Ni values are also elevated in the examined sections. At Mud Buttes the peak occurs at the top of the mudstone layer with the Ni-anomaly at 129.5 ±18 ppm. At John's Nose on the other hand, a peak that may or may not be linked to the K–Pg boundary event occur in the overlaying coal layer at 295 ±24 ppm.

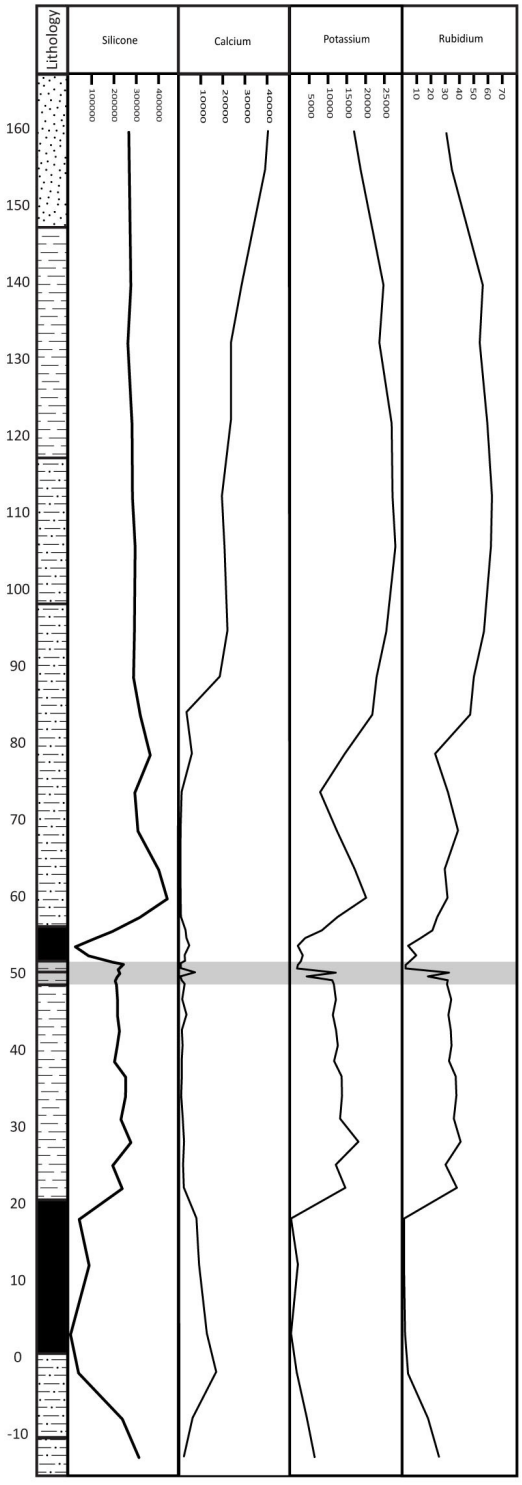

Fig. 10. Elements increasing in the upper meter of John's Nose section. Displayed elements are Si, Ca, K and Rb, all values are given in ppm.

Like Cr, the Ni correlation measurements demonstrate a relatively big difference from the standard reference placing the values 83-104% above it. These results might indicate that the Ni values measured are in fact lower in reality. Comparing the results to measurements in Stevns Klint at 1137 ppm (Alvarez et al. 1980), Gubbio at 176.8 ppm (Smit & ten Kate1982)

Table 2. Comparison of geochemistry measured at the K–Pg boundary layers at Mud Buttes, John's Nose, Stevns Klint, Gubbio, Sugarite and Belize-Mexico. All values are given in ppm.

Element (ppm)	Mud Buttes	John's Nose	Stevns Klint (Alvarez et al. 1980)	Gubbio (Smit &ten Kate 1982)	Sugarite (Gilmore et al. 1984)	Belize-Mexico (Wigforss-Lange et al. 2007)
Ti	11200.9	42594.5		4608	13500	
Cr	275.7	291.1	371	178.5	100	
Ni	129.5	295.3	1137	179.8	50	
As	301.7	333.8	96			14.9

and Sugarite at 50 ppm (Gilmore et al. 1984) show a big spread ranging from 50-1137 ppm. These differences may derive form physical factors at or after the deposition.

The Ti value measured in this study shows a peak in the K–Pg boundary spherule layer at both localities while remaining relatively stable in the rest of the samples. The highest peak is 11201 ±127 ppm at Mud buttes and 42595 ±68 ppm at John's Nose. For Mud Buttes this value is approximately 230 % higher than the average value above and below the boundary at 4355 ±63 ppm and for John's Nose the value is 1120% higher than the average value above and below the boundary at 3689 ±67 making it a distinct elevation at the K–Pg event. Ti levels measured with neutron activation analysis and insoluble residue determination in K–Pg boundary deposits in Gubbio, Italy show a value of 4608 ppm (Smit & ten Kate 1982). This value is apparently much lower than measured values at both John's Nose and Mud Buttes sections and more coherent with the average value among samples above and below the K–Pg boundary. On the other hand, Ti values at another section in Sugarite, USA, also measured with neutron activation analysis show values at 13500 ppm (Gilmore et al. 1984) which is fairly close to the peak value measured at Mud Buttes at 11201 ±127 ppm. The peak value at 42595 ±67 ppm in John's Nose is very high compared to Mud Buttes and the sections in Denmark and USA mentioned above. The sources of error show good precision and no drift in the Ti correlation samples could account for these high concentrations.

Sulphur is elevated in a couple of samples at both locations. High values seen in sample 175HC3 to 175FU4 and 175FU22 to 175FU25 at John's Nose section are situated in coal layers (Fig. 8). These elevations can be explained by coal forming processes. An elevation is also detected at the K–Pg boundary in the Ir-anomaly layer at Mud Buttes at 26408 ±221 and in the spherule layer at John's Nose at 17015 ±179. At both locations the peak in S in the same sample corresponds to a peak in Ca at 16258 ±289 ppm in Mud Buttes and 7137 ±106 in John's Nose. High values of S and CaO in K–Pg boundary tektites have earlier been measured in Haiti with up to 0.4% S and 20% Ca (Izett 1991; Sigurdsson et al. 1991). This indicates that the elevation of S and Ca is not a local phenomenon but a consequence of contribution from the carbonate platform in Yucatán.

Measured values of As is notably high in the K–Pg boundary layer peaking at 302 ±10 ppm in the spherule layer at Mud Buttes and at 334 ±13 ppm in the spherule layer at John's Nose. These peaks represent an elevation of approximately 8–10 times the average value under and above the K–Pg boundary layer. Previous measurements preformed at the Belize-Mexico border shows elevated values at up to 14.9 ppm (Wigforss-Lange et al. 2007) and in Stevns Klint a value at 96 ppm (Alvarez et al. 1980) was measured. These values are far below the values measured in the peaks at the K–Pg boundary in Mud Buttes and John's Nose in up to 334 ppm. Calibration samples show results up to 224% higher than the standard suggesting that the measured value is above reality. This might influence the measured element concentration overall but not the relative elevations seen at the K–Pg boundary.

Variations seen between different locations may be related to differences in biological, hydrological or geological conditions during deposition. Furthermore, different analyse methods can provide slightly different accuracy. Nonetheless, the measured geochemical trends of the sections analysed in this study generally concur with those of other sections from this time interval elsewhere in the world (Table 2).

6. Conclusion

The values measured and discussed in this study show signs of a depositional difference at the K–Pg boundary that correlate fairly well to values and very well to the trends measured with different methods elsewhere. This indicates that anomalies seen at the boundary is in fact related to the K–Pg event and thus the portable XRF device has been able to detect it. Among the elevated elements at the boundary several can be associated with meteorites or the Chicxulub impact area. Elevated values of Cr, Ni, Ti, S, Ca and As among others are good markers for the K–Pg boundary when using portable XRF in this kind of depositional environment.

This present work demonstrates that portable XRF devices can be an excellent tool for fast and easy detection of the K–Pg boundary. Combining this with its portability makes it applicable in both laboratory uses and fieldwork.

7. Acknowledgements

First of all I would like to thank my supervisor Antoine Bercovici for all the help and support throughout this project. Olof Peterffy and Ludvig Ehlorsson are thanked for help with text corrections. Dean Pearson at Pioneer Trails Regional Museum (Bowman, ND) is thanked for assistance in the field. Additionally I am grateful for all encouragement and support from my lovely family and friends.

8. References

Alvarez, L.W., Alvarez, W., Asaro, F. & Michel, H.V., 1980: Extraterrestrial cause for the Cretaceous – Tertiary extinction. *Science 208,* 1095–1108.

Arai, T., 2006: Introduction. *In* Backhoff, B., Kangnießer, B., Langhoff, N., Wedell, R. & Wolff, H. (eds): *Handbook for practical fluorescence analysis*, 1–31. Springer Berlin Heidelberg.

Barker, J.L. & Anders, E., 1968: Accretion rate of cosmic matter from iridium and osmium contents of deep-sea sediments. *Ceochimica et Cosmochimica Acta 32,* 627–645.

Bercovici, A., Pearson, D., Nichels, D. & Wood, J., 2009: Biostratigraphy of selected K/T boundary sections in southwestern North Dakota, USA: toward a refinement of palynological identification criteria. *Cretaceous Research 30,* 632–658.

Bercovici, A., Vajda, V., Pearson, D., Villanueva-Amadoz, U. & Kline, D., 2012: Palynostratigraphy of John's Nose, a new Cretaceous–Paleogene boundary section in southwestern North Dakota, USA. *Palynology 36,* 36–47.

Brett, R., 1992: The Cretaceous-Tertiary extinction: A lethal mechanism involving anhydrite target rocks. *Geochimica et Cosmochimica Acta 56,* 3603–3606.

Brouwer, P., 2010: *Theory of XRF: Getting aquainted with the principles.* PANalytical BV. pp 59.

Crocket, J.H. & Kuo, H.Y., 1979: Sources for gold, palladium and iridium in deep-sea sediments. *Geochimica et Cosmochimica Acta 43,* 831–842.

Gilmore, J.S., Knight, J.D., Orth, C.J., Pillmore, C.L. & Tschudy, R.H., 1984: Trace element patterns at a non-marine Cretaceous–Tertiary boundary. *Nature 307,* 224–228.

Hammond, C.R. 2012: Section 4: The elements. *In* Haynes, W.M., Lide, D.R. & Bruno, T.J. (eds.): *Handbook of chemistry and physics, 93rd edition*. 1–42, Taylor Francis group LLC.

Hildebrand, A.H., Penfield, G.T., Kring, D.A., Pilkington, M., Camargo Z.A., Jacobsen, S.B. & Boynton, V., 1991: Chicxulub crater: A possible Cretaceous/Tertiary boundary impact crater on the Yucatán Peninsula, Mexico. *Geology 19,* 867–871.

Izett, G.A., 1990: The Cretaceous/Tertiary boundary interval, Raton Basin, Colorado and New Mexico, and its content of shock-metamorphosed minerals; Evidence relevant to the K/T boundary impact-extinction theory. *The Geological Society of America Special Paper 249*. 100 pp.

Izett, G.A., 1991: Tektites in Cretaceous-Tertiary boundary rocks on Haiti and their bearing on the Alvarez impact extinction hypothesis. *Journal of geophysical research 96,* 20879–20905.

Johnson, K.R., Nichols, D.J. & Hartman, J. H., 2002: Hell creek formation: A 2001 synthesis. *In* Hartman, J.H., Johnson, K.R. & Nichols,D.J. (eds.): *The Hell Creek formation and the Cretaceous-Tertiary boundary in the Northern Great Plains: an integrated continental record of the end of the Cretaceous,* 503–510. Geological society of America Special Paper 321.

Kring, D.A., 2007: The Chicxulub impact event and its environmental consequences at the Cretaceous–Tertiary boundary. *Palaeogeography, Palaeoclimatiology, Palaeoecology 255*, 4–21.

Lerbekmo, J.F., Sweet, A.R. & Davidson, R.A., 1999: Geochemistry of the Cretaceous–Tertiary (K-T) boundary interval: south-central Saskatchewan and Montana. *Canadian Journal of Earth Sciences 36,* 717–724.

Moore, C.B. & Brown, H., 1961: The distribution of manganese and titanium in stony meteorites. *Geochemica et Cosmochimica Acta 26,* 495–502.

Nichols, D.J. & Johnson, K.R., 2008: *Plants and the K–Pg boundary.* Cambridge university press. 280 pp.

Renne, P.R.,Deino, A.L., Hilgen, F.J., Kuiper, K.F., Mark, D.F., Mitchell III, W.S., Morgan, L.E., Mundil, Rb & Smit, J., 2013: Time Scales of critical events around the Cretaceous-Paleogene boundary. *Science 8,* 684–687.

Schulte, P., Alegret, L., Arnillas, I., Arz, J.A., Barton, P.J., Bown, P.R., Bralower, T.J., Christeson, G.L., Claeys, P., Cockell, C.S., Collins, G.S., Deutsch, A., Goldin, T.J., Goto, K., Grajales-Nishimura, J.M., Grieve, R.A.F., Gulick, S.P.S., Johnson, K.R., Kiessling, W., Kobeberl, C., Kring, D.A., MacLeod, K.G., Matsui, T., Melosh, J., Montanari, A., Morgan, J.V., Neal, C.R., Nichols, D.J., Norris, R.D., Pierazzo, E., Ravizza, G.,Rebolledo-Vieyra, M., Reimond, W.U., Robin, E., Salge, T., Speijer, R.P., Sweet, A.R., Urrutia-Fucugauchi, J., Vajda, V., Whalen, M.T. & Willumsen, P.S., 2010: The Chicxulub asteroid impact and the mass extinction at the Cretaceous-Paleogene boundary. *Science 327,* 1214–1218.

Sigurdsson, H., D´Hondt, S., Arthur, M.A., Bralower, T.J., Zachos, J.C., van Fossen, M. & Channell, J.E.T., 1991: Glass from the Cretaceous/Tertiary boundary in Haiti. *Nature 349,* 482–487.

Smit, J. & ten Kate, W.G.H.Z., 1982: Trace-element patterns at the Cretaceous-Tertiary boundary – consequences of a large impact. *Cretaceous Research 3,* 307–332.

Sweet, A.R., Braman, D.R. & Lerbekmo, J.F., 1999: Sequential palynological changes across the composite Cretaceous-Tertiary (K-T) boundary claystone and contiguous strata, western Canada and Montana, U.S.A. *Canadian Journal of Earth Sci-*

ences 36, 743–768.
Tuchscherer, M.G., Reimold, W.U., Koeberl, C. & Gibson, R.L., 2005: Geochemical and petrographic characteristics of impactites and Cretaceous target rocks from the Yaxcopoil-1 borehole, Chicxulub impact structure, Mexico: Implications for target composition. *Meteoritics & Planetary Science 40,* 1513–1536.
Vajda, V., Raine, I. & Hollis, C., 2001: Indication of a global deforestation at the Cretaceous–Tertiary boundary by New Zealand fern spike. *Science 294*, 1700–1702.
Ward, W. C., Keller, W., Stinnesbeck, W. & Adatte, T., 1995: Yucatán subsurface stratigraphy: Implications and constrains for the Chicxulub impact. *Geology 23,* 873–876.
Wigforss-Lange, J., Vajda, V. & Ocampo, A., 2007: Trace element concentrations in the Mexico-Belize ejecta layer: A link between the Chicxulub impact and the global Cretaceous-Paleogene boundary. *Meteoritics & Planetary Science 42,* 1871–1882.

9. Appendix

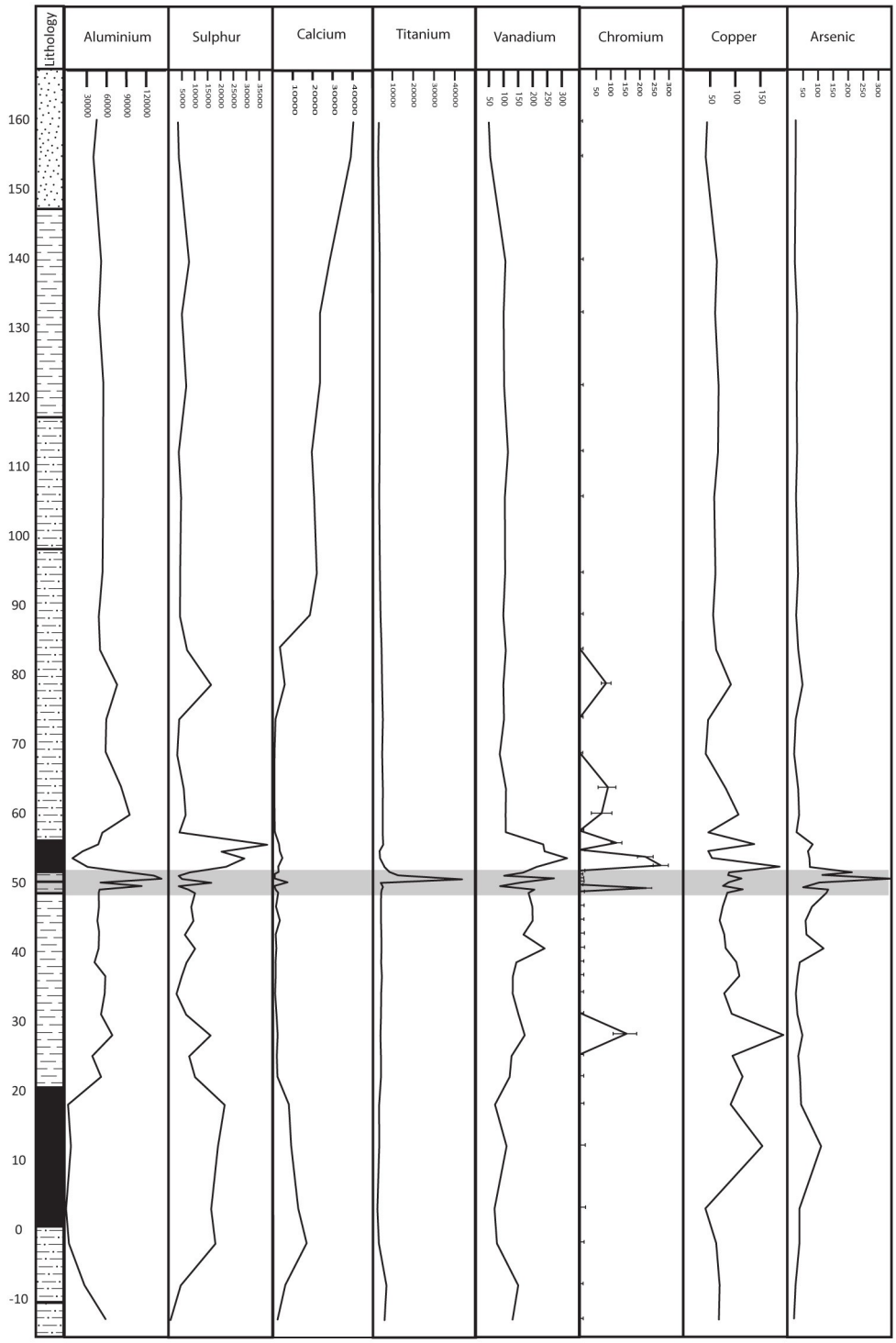

Appendix Fig. 1. Plots displaying elevated element values at or just above the K–Pg boundary at John's Nose section. Displayed elements are Al, S, Ca, Ti, V, Cr, Cu and As. The K–Pg boundary interval is marked with grey. All values given in ppm.

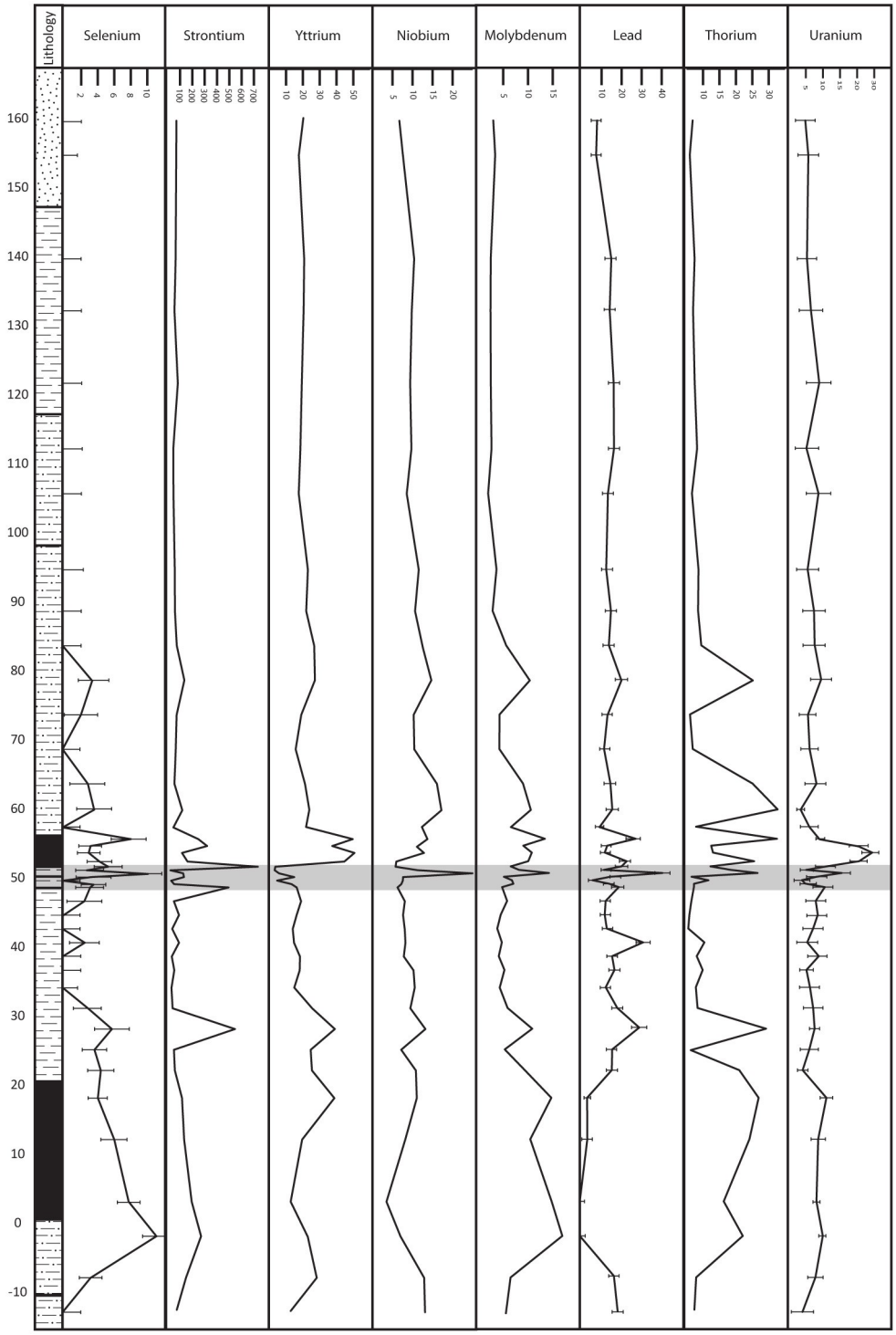

Appendix Fig. 2. Plots displaying elevated element values at or just above the K–Pg boundary at John's Nose section. Displayed elements are Se, Sr, Y, Nb, Mo, Pb, Th and U. The K–Pg boundary interval is marked with grey. All values given in ppm.

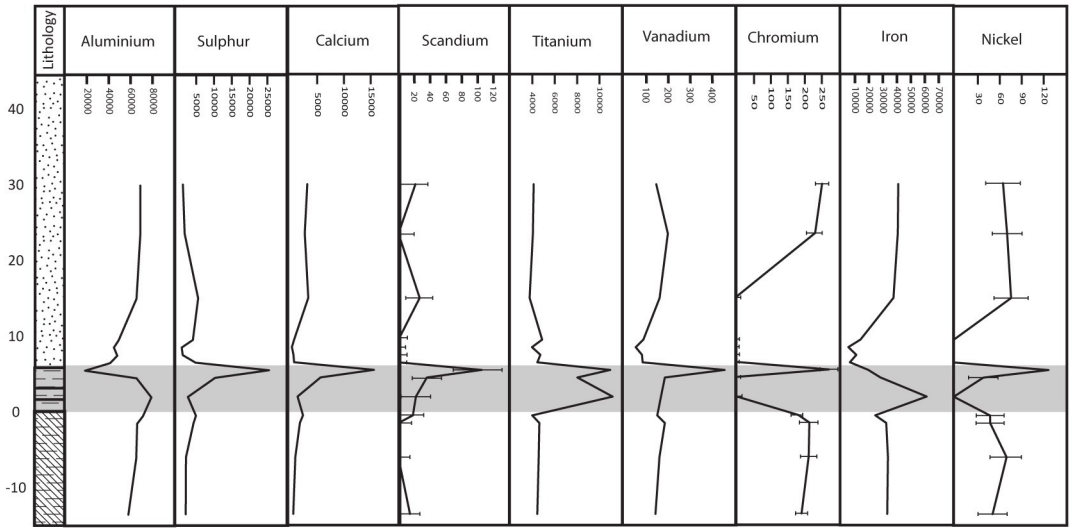

Appendix Fig. 3. Plots displaying elevated element values at or just above the K–Pg boundary at Mud Buttes section. Displayed elements are Al, S, Ca, Sc, Ti, V, Th, Fe and Ni.. The K–Pg boundary interval is marked with grey. All values given in ppm.

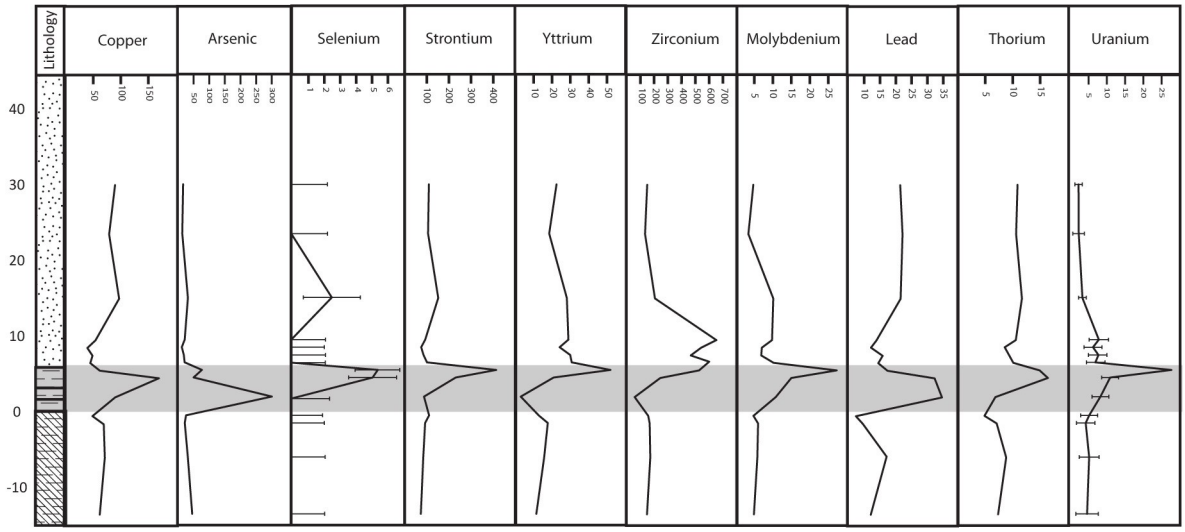

Appendix Fig. 4. Plots displaying elevated element values at or just above the K–Pg boundary at Mud Buttes section. Displayed elements are Cu, As, Se, Sr, Y, Zr, Mo, Pb, Th and U. The K–Pg boundary interval is marked with grey. All values given in ppm.

Appendix Table 1. All detected values measured at John's Nose section in this study. Elements below the detection limit (<LOD) ranges between 0 and the displayed error. All values given in ppm.

SAMPLE	Ti	Ti Error	V	V Error	Cr	Cr Error	Mn	Mn Error
175HC1	5375.73	62.39	130.87	17.30	< LOD	12.77	500.82	34.91
175HC2	6278.76	64.00	150.37	17.78	< LOD	12.27	< LOD	27.48
175HC3	2650.45	55.13	77.27	17.55	< LOD	15.92	< LOD	22.48
175FU1	1915.61	59.50	68.96	16.79	< LOD	21.07	< LOD	24.62
175FU2	2797.03	67.66	110.44	28.16	< LOD	20.18	< LOD	33.84
175FU3	2747.65	52.99	70.64	18.09	< LOD	15.61	< LOD	23.62
175FU4	3442.39	57.10	121.02	16.83	< LOD	14.14	< LOD	35.05
175FU5	3632.34	58.37	127.40	17.18	< LOD	14.04	< LOD	32.94
175FU6	3402.19	82.11	172.65	25.72	168.61	42.94	59.92	39.81
175FU7	3671.84	60.07	151.10	20.08	< LOD	14.62	< LOD	34.24
175FU8	3715.09	57.98	131.35	19.21	< LOD	13.80	< LOD	35.19
175FU9	4092.64	63.69	131.96	18.49	< LOD	14.80	< LOD	35.64
175FU10	3718.90	60.90	144.04	19.73	< LOD	14.83	< LOD	35.49
175FU11	3885.29	71.26	240.89	31.00	< LOD	17.57	< LOD	41.82
175FU12	3817.84	66.44	168.43	21.78	< LOD	16.28	< LOD	38.64
175FU13	3654.80	63.52	199.83	25.14	< LOD	15.65	< LOD	35.99
175FU14	3651.85	64.43	198.91	23.95	< LOD	16.42	< LOD	36.32
175FU15	3708.15	78.15	185.70	24.19	< LOD	17.16	< LOD	41.64
175FU16	3973.80	70.14	205.64	21.40	238.02	22.96	< LOD	37.71
175FU17	4601.20	52.21	87.96	16.20	< LOD	11.31	< LOD	28.11
175FU18	3539.31	68.04	159.67	20.68	< LOD	16.13	< LOD	37.12
175FU19	42594.54	254.46	281.96	39.54	< LOD	14.41	< LOD	33.72
175FU20	11840.13	106.69	102.11	18.93	< LOD	11.78	< LOD	28.95
175FU21	7736.70	84.78	166.86	32.08	< LOD	15.31	< LOD	35.42
175FU22	5379.46	76.51	213.34	22.52	291.06	27.29	< LOD	30.96
175FU23	3194.53	83.70	318.08	28.10	235.58	28.42	< LOD	32.32
175FU24	2955.99	70.41	240.76	23.02	< LOD	19.57	< LOD	32.26
175FU25	4698.01	79.65	236.15	24.36	131.67	20.02	< LOD	42.45
175FU26	4467.22	55.35	107.64	15.54	< LOD	11.89	< LOD	31.72
175FU27	4494.14	54.96	107.15	15.42	78.64	37.46	< LOD	39.91
175FU28	4555.50	55.35	108.32	15.47	101.52	32.43	< LOD	36.06
175FU29	4217.23	51.32	86.94	14.34	< LOD	11.11	< LOD	31.69
175FU30	4552.61	55.97	101.51	15.60	< LOD	12.08	75.27	25.23
175FU31	4191.45	54.76	99.45	15.33	95.05	17.53	385.69	36.33
175FU32	3942.36	57.89	107.65	16.59	< LOD	12.92	< LOD	36.75
175FU33	3434.44	56.22	99.12	16.21	< LOD	12.93	66.39	26.95
175FU34	3140.08	55.89	105.37	16.36	< LOD	13.16	51.78	26.76
175FU35	2785.28	53.10	104.41	15.76	< LOD	12.90	91.27	28.04
175FU36	2964.17	55.28	115.15	18.97	< LOD	13.20	113.25	29.24
175FU37	3027.61	57.90	102.03	17.09	< LOD	13.34	131.38	29.20
175FU38	2982.88	54.15	100.29	15.86	< LOD	12.91	198.60	31.01
175FU39	3052.13	54.33	106.50	15.90	< LOD	12.90	119.21	28.47
175FU40	2275.84	44.15	54.43	12.70	< LOD	10.61	121.75	28.29
175FU41	2613.09	45.17	49.43	12.71	< LOD	10.17	98.88	27.35

SAMPLE	Fe	Fe Error	Ni	Ni Error	Cu	Cu Error	Zn	Zn Error
175HC1	21068.42	173.31	< LOD	20.92	70.71	8.77	33.62	4.78
175HC2	5231.80	62.69	< LOD	18.13	72.11	8.20	28.14	4.04
175HC3	4120.31	50.98	< LOD	15.58	65.34	7.40	15.56	3.48
175FU1	19807.66	147.74	< LOD	15.47	43.78	6.97	< LOD	4.75
175FU2	46154.95	252.02	< LOD	19.50	157.33	10.06	7.36	5.59
175FU3	5029.74	55.50	< LOD	16.54	94.11	7.95	49.31	4.13
175FU4	28679.33	206.19	< LOD	22.05	117.88	9.97	142.09	7.36
175FU5	22597.90	174.53	< LOD	21.68	97.75	9.12	98.88	6.07
175FU6	39012.27	274.19	145.99	22.81	199.20	13.20	185.26	9.53
175FU7	27250.53	195.86	< LOD	21.15	101.19	9.37	119.40	6.71
175FU8	28426.76	202.03	< LOD	21.09	81.26	8.98	116.95	6.72
175FU9	31336.55	213.54	< LOD	21.51	111.57	9.71	116.06	6.80
175FU10	28679.18	200.65	< LOD	20.94	105.49	9.44	80.51	5.88
175FU11	51517.93	290.82	< LOD	23.10	84.25	9.34	82.58	7.18
175FU12	36972.94	236.70	< LOD	21.95	81.36	9.13	76.26	6.10
175FU13	32978.92	218.66	< LOD	21.26	72.22	8.75	68.94	5.76
175FU14	35966.17	228.74	< LOD	21.30	78.30	8.87	66.05	5.74
175FU15	36738.53	244.43	36.53	20.26	87.59	9.66	74.09	6.49
175FU16	39569.41	243.58	< LOD	21.81	118.07	9.88	76.45	6.65
175FU17	14105.35	136.35	< LOD	18.70	78.87	8.57	34.63	4.42
175FU18	33420.07	223.24	< LOD	21.87	90.35	9.28	70.44	5.90
175FU19	27383.31	208.90	< LOD	22.40	115.62	10.14	26.35	4.98
175FU20	15862.25	149.43	< LOD	19.84	89.12	9.11	48.19	5.03
175FU21	31548.17	215.06	< LOD	21.28	90.97	9.27	42.52	5.20
175FU22	26352.89	181.54	102.72	18.04	191.65	10.64	29.12	4.37
175FU23	35377.51	210.49	111.41	18.02	56.76	7.86	15.46	4.65
175FU24	29543.83	197.84	58.07	17.82	49.47	7.93	18.43	4.35
175FU25	39402.83	266.56	295.32	24.22	141.13	11.63	43.60	6.15
175FU26	15633.97	147.78	< LOD	20.21	49.59	8.17	23.68	4.35
175FU27	24622.50	214.66	< LOD	26.33	109.77	11.22	35.41	5.99
175FU28	22653.77	194.62	< LOD	23.66	84.58	9.92	26.92	5.21
175FU29	12391.01	130.52	< LOD	20.00	44.45	7.97	16.93	4.00
175FU30	15435.43	147.69	< LOD	20.81	49.18	8.24	23.80	4.34
175FU31	25058.20	206.80	148.25	21.66	94.60	10.33	90.64	6.96
175FU32	23962.36	187.85	48.50	21.10	65.24	8.78	54.20	5.42
175FU33	23368.88	188.42	58.15	19.07	59.15	8.75	57.36	5.57
175FU34	26153.12	200.17	< LOD	22.49	63.78	8.82	64.48	5.79
175FU35	25687.29	199.73	48.84	19.91	61.38	8.84	59.22	5.70
175FU36	27239.08	208.89	54.08	19.35	68.94	9.18	68.78	6.05
175FU37	26596.23	203.94	49.95	19.98	70.18	9.07	62.68	5.82
175FU38	25113.57	199.35	63.13	19.47	63.10	9.00	55.71	5.65
175FU39	25513.70	198.19	< LOD	22.38	66.65	8.89	51.53	5.47
175FU40	14700.44	152.93	47.98	24.68	44.40	8.56	28.71	4.77
175FU41	12572.90	140.52	35.76	21.37	47.13	8.58	25.23	4.60

SAMPLE	As	As Error	Se	Se Error	Rb	Rb Error	Sr	Sr Error
175HC1	10.44	5.45	< LOD	2.10	26.02	1.00	94.01	2.09
175HC2	15.47	5.13	3.39	1.33	18.36	1.20	168.91	2.53
175HC3	28.30	4.02	11.34	1.37	4.35	0.85	291.41	3.01
175FU1	28.31	3.73	7.99	1.29	2.23	0.82	215.18	2.67
175FU2	100.38	6.27	6.25	1.50	1.54	1.21	153.78	2.51
175FU3	33.88	4.11	4.26	1.18	1.61	0.72	136.61	2.07
175FU4	30.43	5.79	4.62	1.57	38.59	1.19	78.34	1.95
175FU5	24.47	5.49	3.85	1.42	30.64	1.03	71.04	1.78
175FU6	38.18	7.80	5.96	1.99	41.22	1.45	567.06	5.69
175FU7	21.59	5.67	3.07	1.62	36.45	1.13	60.14	1.69
175FU8	16.46	5.18	< LOD	2.10	38.26	1.16	50.80	1.59
175FU9	22.19	5.63	< LOD	2.16	37.76	1.17	73.81	1.88
175FU10	29.38	5.68	< LOD	2.05	33.09	1.09	53.30	1.61
175FU11	108.64	8.55	2.68	1.76	34.85	1.17	112.19	2.38
175FU12	51.73	6.25	< LOD	2.14	34.31	1.14	56.85	1.71
175FU13	48.72	6.06	< LOD	2.11	32.67	1.10	112.06	2.26
175FU14	69.88	6.50	2.63	1.96	34.62	1.12	70.48	1.84
175FU15	118.03	8.39	3.34	1.62	31.68	1.19	514.66	4.98
175FU16	123.87	7.84	3.27	1.54	32.17	1.10	72.31	1.88
175FU17	40.63	5.06	< LOD	1.90	18.31	1.19	48.07	1.48
175FU18	94.65	7.30	3.45	2.03	33.04	1.12	152.33	2.65
175FU19	333.79	12.53	10.32	1.89	2.62	1.01	146.12	2.69
175FU20	104.25	7.10	2.93	1.61	2.65	0.83	42.21	1.45
175FU21	202.43	9.57	5.51	1.62	5.68	1.14	753.09	5.72
175FU22	63.10	6.57	4.46	1.39	10.09	1.11	181.25	2.63
175FU23	61.62	5.81	3.16	1.29	4.39	0.98	136.23	2.28
175FU24	56.70	6.03	3.38	1.37	13.20	1.23	340.66	3.67
175FU25	72.32	8.20	8.26	1.97	21.43	1.64	268.75	3.81
175FU26	18.72	4.96	< LOD	2.05	24.82	1.17	66.38	1.77
175FU27	27.20	6.55	3.82	2.15	32.03	1.26	138.88	2.91
175FU28	24.20	6.02	3.06	2.10	30.08	1.15	74.87	2.06
175FU29	10.84	4.36	< LOD	2.03	39.38	1.64	85.56	1.95
175FU30	15.98	5.20	2.22	1.94	32.32	1.54	92.83	2.06
175FU31	38.62	6.89	3.58	1.75	23.33	1.06	155.54	2.90
175FU32	24.43	5.63	< LOD	2.13	47.90	1.31	94.07	2.13
175FU33	17.53	5.54	< LOD	2.15	50.49	1.35	78.91	1.99
175FU34	23.79	5.53	< LOD	2.13	57.58	1.44	77.71	1.98
175FU35	16.94	5.48	< LOD	2.16	62.48	1.51	66.84	1.87
175FU36	20.44	5.87	< LOD	2.26	63.23	1.54	65.56	1.88
175FU37	19.22	5.75	< LOD	2.20	59.97	1.48	102.43	2.26
175FU38	20.46	5.70	< LOD	2.18	54.61	1.43	75.10	1.98
175FU39	12.93	5.42	< LOD	2.14	56.76	1.43	84.63	2.06
175FU40	15.89	5.04	< LOD	2.17	35.13	1.18	89.82	2.16
175FU41	15.89	5.03	< LOD	2.17	31.24	1.11	91.20	2.15

SAMPLE	Y	Y Error	Zr	Zr Error	Nb	Nb Error	Mo	Mo Error
175HC1	12.73	1.36	222.93	3.17	13.37	1.18	5.74	1.30
175HC2	28.24	1.40	237.06	3.06	12.91	1.12	6.68	1.23
175HC3	22.91	1.16	50.60	1.81	7.00	1.00	17.11	1.36
175FU1	12.72	1.03	23.90	1.54	3.51	1.00	14.95	1.36
175FU2	19.54	1.24	78.58	2.12	8.20	1.09	10.65	1.24
175FU3	38.75	1.33	62.54	1.70	11.08	1.02	14.89	1.12
175FU4	25.39	1.61	142.18	2.66	10.85	1.19	9.55	1.32
175FU5	24.63	1.50	145.19	2.55	7.18	1.09	5.51	1.22
175FU6	39.03	2.07	176.03	3.84	13.23	1.46	11.05	1.57
175FU7	25.53	1.57	168.75	2.76	9.47	1.14	6.08	1.27
175FU8	14.85	1.44	143.98	2.61	10.57	1.15	4.50	1.25
175FU9	18.09	1.50	154.99	2.73	10.26	1.16	5.45	1.28
175FU10	18.26	1.45	149.91	2.62	7.84	1.11	4.31	1.24
175FU11	14.70	1.50	149.40	2.85	8.25	1.17	4.93	1.31
175FU12	13.95	1.44	145.83	2.68	8.06	1.14	4.00	1.27
175FU13	16.26	1.44	156.60	2.76	7.65	1.12	4.70	1.26
175FU14	18.92	1.48	170.07	2.81	8.09	1.13	5.99	1.29
175FU15	16.30	1.54	199.92	3.61	6.26	1.20	4.98	1.38
175FU16	13.25	1.41	183.69	2.95	7.22	1.12	7.25	1.32
175FU17	4.62	1.05	55.53	1.76	7.60	1.04	6.96	1.16
175FU18	14.82	1.44	177.13	2.98	7.65	1.13	5.34	1.30
175FU19	5.77	1.15	75.45	2.32	24.98	1.39	14.41	1.70
175FU20	3.17	1.00	45.05	1.70	11.33	1.12	8.39	1.28
175FU21	3.55	1.10	78.45	2.93	5.78	1.11	6.72	1.27
175FU22	44.68	1.60	305.23	3.43	5.97	1.10	10.24	1.33
175FU23	50.70	1.62	209.82	2.88	12.87	1.18	10.96	1.29
175FU24	37.48	1.55	214.49	3.19	11.11	1.18	9.24	1.32
175FU25	49.71	2.00	365.77	4.51	13.74	1.43	13.59	1.65
175FU26	21.86	1.46	308.13	3.57	12.35	1.17	6.74	1.34
175FU27	23.82	1.79	319.69	4.35	17.23	1.46	10.76	1.63
175FU28	21.24	1.64	333.72	4.11	16.11	1.34	9.19	1.52
175FU29	15.68	1.36	319.94	3.59	10.45	1.12	4.42	1.31
175FU30	19.03	1.41	354.34	3.83	10.30	1.14	4.47	1.35
175FU31	27.16	1.71	382.13	4.46	14.71	1.35	10.56	1.58
175FU32	26.72	1.69	254.66	3.41	12.58	1.22	5.80	1.35
175FU33	21.97	1.65	191.93	3.05	10.65	1.20	3.06	1.30
175FU34	22.96	1.70	171.05	2.92	11.57	1.21	3.85	1.29
175FU35	17.51	1.66	124.20	2.58	8.57	1.17	2.17	1.68
175FU36	18.50	1.71	136.82	2.72	9.73	1.20	2.85	1.53
175FU37	19.34	1.68	149.62	2.82	9.42	1.19	2.70	1.28
175FU38	20.42	1.68	174.98	2.99	9.82	1.20	2.65	1.52
175FU39	20.76	1.67	185.78	3.03	10.42	1.19	2.69	1.29
175FU40	17.57	1.55	320.34	3.89	7.62	1.17	3.58	1.40
175FU41	20.28	1.56	337.77	3.95	6.72	1.15	3.20	1.39

SAMPLE	W	W Error	Hg	Hg Error	Pb	Pb Error	Th	Th Error
175HC1	91.52	23.59	< LOD	5.77	18.91	2.73	8.67	1.82
175HC2	< LOD	14.16	5.10	4.69	17.03	2.46	9.21	1.63
175HC3	< LOD	12.28	180.23	5.89	< LOD	2.57	23.42	3.67
175FU1	< LOD	11.52	97.88	4.77	< LOD	2.26	17.60	3.57
175FU2	146.21	18.72	< LOD	5.39	3.76	2.57	25.44	3.93
175FU3	111.24	16.18	13.53	3.26	3.65	1.66	28.24	3.51
175FU4	145.51	19.42	< LOD	6.09	15.98	2.68	22.35	4.04
175FU5	< LOD	14.94	< LOD	5.32	16.18	2.54	7.57	1.71
175FU6	299.74	33.60	10.86	6.64	29.69	3.74	30.51	5.45
175FU7	82.21	18.05	< LOD	5.64	18.72	2.71	9.64	1.86
175FU8	< LOD	16.01	< LOD	5.59	12.93	2.47	9.11	1.85
175FU9	< LOD	16.37	< LOD	5.79	17.32	2.69	11.20	1.96
175FU10	< LOD	15.49	< LOD	5.48	16.12	2.57	9.38	1.83
175FU11	< LOD	17.03	6.48	5.65	31.62	3.36	11.72	3.05
175FU12	80.04	18.20	5.92	5.38	13.49	2.54	6.82	1.84
175FU13	< LOD	15.91	< LOD	5.69	12.45	2.46	7.15	1.80
175FU14	< LOD	16.07	< LOD	5.74	12.91	2.48	7.76	1.83
175FU15	< LOD	17.02	7.60	5.15	19.48	2.99	8.53	2.05
175FU16	< LOD	16.42	< LOD	5.79	14.78	2.62	8.56	1.90
175FU17	< LOD	14.79	< LOD	5.25	6.39	2.00	12.95	3.06
175FU18	< LOD	16.47	< LOD	5.76	15.21	2.63	7.79	1.86
175FU19	171.07	22.05	< LOD	6.45	41.26	3.72	27.91	3.78
175FU20	109.92	17.94	< LOD	5.71	11.98	2.36	19.79	3.77
175FU21	< LOD	16.04	6.40	5.38	20.84	2.94	13.56	4.70
175FU22	101.74	16.43	8.94	3.62	23.40	2.76	26.87	4.06
175FU23	< LOD	14.02	8.08	3.42	12.48	2.25	14.34	3.77
175FU24	< LOD	14.67	17.32	3.85	13.69	2.41	13.78	4.12
175FU25	381.59	32.05	35.18	5.79	27.92	3.52	33.83	5.07
175FU26	125.27	21.55	8.18	4.45	9.85	2.31	9.18	1.76
175FU27	336.49	33.01	< LOD	8.08	16.24	3.12	34.03	5.03
175FU28	234.94	28.68	< LOD	7.04	15.29	2.86	26.37	3.94
175FU29	78.59	18.98	< LOD	5.52	12.11	2.38	8.17	1.70
175FU30	< LOD	15.89	< LOD	5.60	13.83	2.50	7.34	1.71
175FU31	234.21	29.67	8.31	6.62	20.79	3.14	26.48	4.72
175FU32	< LOD	16.70	< LOD	5.93	14.52	2.61	10.77	1.96
175FU33	92.90	22.75	< LOD	6.05	15.55	2.68	9.80	1.96
175FU34	105.19	18.89	< LOD	6.07	13.19	2.59	9.92	1.99
175FU35	117.00	21.13	< LOD	6.09	14.06	2.64	7.93	1.94
175FU36	94.31	19.57	< LOD	6.22	17.08	2.83	9.51	2.04
175FU37	89.05	21.23	< LOD	6.19	16.91	2.78	8.77	1.98
175FU38	96.79	21.29	< LOD	6.21	14.92	2.70	8.26	1.95
175FU39	102.20	18.87	7.29	5.61	15.72	2.70	8.73	1.95
175FU40	93.20	19.17	< LOD	6.17	8.17	2.38	7.27	1.83
175FU41	84.43	18.98	< LOD	6.09	8.64	2.39	8.14	1.84

SAMPLE	U	U Error	Mg	Mg Error	Al	Al Error	Si	Si Error
175HC1	4.31	3.21	10243.71	3600.20	63187.54	1510.99	318898.9	1447.08
175HC2	8.10	2.20	7113.06	3236.44	31250.72	931.98	244502.4	1268.08
175HC3	10.24	1.00	8206.16	2649.68	7677.61	553.43	47971.52	629.28
175FU1	8.39	1.00	5783.25	2702.31	3407.72	401.99	12181.10	320.60
175FU2	8.90	2.07	9888.14	3447.25	10726.85	746.32	95441.77	935.24
175FU3	11.30	1.84	5749.12	2585.79	6385.99	496.54	51117.63	617.53
175FU4	4.35	1.50	8070.08	4113.03	56454.54	1449.80	243910.5	1331.22
175FU5	6.31	2.61	7702.31	2944.36	43146.60	1090.40	201269.1	1162.09
175FU6	7.86	1.44	15399.31	5254.09	73544.37	2141.03	282782.4	1574.51
175FU7	7.43	2.82	8965.19	3375.44	56373.85	1351.92	238137.6	1269.82
175FU8	6.50	2.85	9188.46	4455.98	61939.70	1483.73	258893.5	1319.76
175FU9	5.47	1.96	11742.79	3607.93	62946.28	1501.60	259675.2	1335.11
175FU10	9.07	2.78	9457.26	3991.57	46550.44	1178.77	209292.1	1185.65
175FU11	5.69	3.00	14319.03	3811.54	52746.91	1412.83	221152.9	1271.15
175FU12	7.42	2.89	11800.02	3359.08	53482.30	1311.72	231464.9	1258.79
175FU13	8.79	2.86	11516.41	3382.69	50893.72	1288.72	222790.7	1241.58
175FU14	8.18	2.86	10452.06	3416.05	53246.26	1329.69	222928.6	1244.15
175FU15	10.83	2.88	13101.54	3537.18	52852.02	1349.91	218380.1	1259.53
175FU16	5.07	2.35	8360.18	3309.17	54168.57	1334.21	212426.3	1229.26
175FU17	4.16	2.27	7906.37	3009.67	117974.2	2039.16	220336.2	1243.87
175FU18	8.44	2.93	12962.28	3801.35	55577.85	1458.34	233304.1	1294.01
175FU19	15.76	2.52	17718.34	4523.37	148066.3	3110.94	225454.5	1420.93
175FU20	5.38	1.90	12502.11	3979.20	136624.8	2509.42	249260.3	1366.15
175FU21	11.40	2.86	9658.49	3253.93	95317.26	1841.06	200772.3	1205.95
175FU22	20.87	2.48	9825.97	2892.03	36029.74	1010.01	93058.63	834.36
175FU23	24.69	2.45	8277.99	2607.46	12975.02	655.87	33843.39	517.40
175FU24	20.73	2.73	9152.42	2766.96	28500.10	883.45	115084.5	900.29
175FU25	9.31	1.28	16594.07	5248.72	52236.27	1794.25	199958.5	1398.90
175FU26	6.36	2.56	8605.56	3639.87	58348.70	1452.25	322632.5	1446.61
175FU27	3.76	1.12	14826.31	5906.01	99817.28	2824.25	445940.6	1733.48
175FU28	8.40	3.03	11055.74	4998.51	86613.56	2295.26	407819.8	1653.79
175FU29	6.40	2.51	7344.96	3360.45	63323.56	1442.93	314508.6	1409.45
175FU30	5.91	2.45	8932.67	4320.49	64285.02	1489.62	300452.8	1391.91
175FU31	9.76	3.01	14878.30	6731.06	80822.16	2331.64	369592.4	1614.28
175FU32	7.86	3.17	14164.64	4175.31	54865.83	1517.90	325259.6	1461.61
175FU33	7.69	3.25	22202.26	4519.99	52988.58	1546.04	294751.5	1440.18
175FU34	5.81	3.18	25880.78	4979.53	58714.81	1740.81	298575.1	1473.80
175FU35	8.99	3.52	24838.13	4921.72	59536.93	1741.99	301927.6	1473.94
175FU36	5.47	3.36	25268.29	4819.54	59571.13	1707.68	289890.3	1452.48
175FU37	9.21	3.52	25140.59	5037.66	59925.92	1783.18	287893.2	1467.75
175FU38	6.79	3.38	24789.32	4672.37	53061.70	1576.78	269121.0	1417.28
175FU39	5.62	2.77	25950.64	5096.42	56649.27	1738.24	282625.7	1454.91
175FU40	6.02	2.98	25111.03	4676.95	44847.53	1441.46	275711.2	1429.14
175FU41	5.12	2.84	21259.79	4548.99	49874.67	1512.02	273582.4	1428.50

SAMPLE	P	P Error	S	S Error	Cl	Cl Error	K	K Error
175HC1	5361.86	230.30	1228.93	55.94	< LOD	54.14	6155.11	119.69
175HC2	3983.02	189.08	5159.66	91.72	< LOD	47.53	4101.22	99.67
175HC3	664.16	120.56	18624.22	173.25	254.44	34.15	1379.33	87.20
175FU1	393.11	91.95	16987.69	152.50	181.10	27.14	< LOD	131.08
175FU2	925.76	154.08	19606.75	195.74	196.81	38.74	1912.06	102.90
175FU3	1254.90	123.45	22227.92	182.93	231.68	31.43	< LOD	98.23
175FU4	5529.66	223.08	10735.33	142.64	< LOD	58.72	14331.55	235.49
175FU5	4014.71	177.27	8437.54	114.23	< LOD	46.95	11782.96	190.42
175FU6	4859.85	278.74	16745.30	210.55	< LOD	79.95	17814.57	298.93
175FU7	5889.36	207.73	7286.38	111.16	< LOD	52.76	12935.41	213.53
175FU8	4883.13	215.08	3520.07	80.60	< LOD	51.57	13448.23	215.51
175FU9	4385.33	208.50	5552.47	100.81	< LOD	53.67	13344.01	223.19
175FU10	4092.83	180.13	7415.80	107.81	< LOD	47.14	11344.42	195.45
175FU11	2630.54	190.83	10742.21	140.12	< LOD	54.62	12330.48	237.59
175FU12	3066.70	184.02	6783.81	106.52	< LOD	49.90	11868.18	213.68
175FU13	2956.38	184.86	10088.95	130.53	< LOD	50.75	11011.98	202.15
175FU14	3712.23	191.43	9238.04	125.62	< LOD	51.46	11820.89	215.54
175FU15	3265.06	188.82	10713.16	136.74	< LOD	51.14	11275.49	210.35
175FU16	3372.20	185.57	8151.88	118.30	< LOD	51.93	10840.04	211.54
175FU17	4409.57	187.61	4392.79	86.13	< LOD	53.80	4061.64	104.62
175FU18	2308.20	197.50	17014.75	178.90	< LOD	55.21	11769.65	213.71
175FU19	2100.55	213.99	5697.49	118.70	< LOD	69.94	1481.52	86.23
175FU20	5680.02	220.62	4390.89	93.15	< LOD	61.63	1672.38	75.69
175FU21	3888.68	184.30	8726.43	121.35	< LOD	52.79	2499.71	98.65
175FU22	2515.39	150.13	22769.93	192.62	72.38	53.75	2990.40	104.00
175FU23	850.16	120.12	29863.81	216.90	215.81	30.15	1671.15	83.15
175FU24	1798.71	143.32	21029.75	181.46	53.82	52.57	3621.29	113.55
175FU25	4015.70	262.11	38723.17	328.98	82.98	97.42	8059.28	205.23
175FU26	7474.74	247.51	4670.50	94.43	< LOD	54.75	12267.18	189.80
175FU27	10722.17	378.12	7067.30	145.38	< LOD	86.29	19869.85	292.91
175FU28	8549.77	325.68	6370.77	128.16	< LOD	75.03	16818.06	254.75
175FU29	7399.89	234.28	3814.78	82.74	< LOD	51.08	12051.79	173.52
175FU30	6478.87	223.44	4574.72	88.72	< LOD	50.26	7623.37	125.71
175FU31	5819.11	306.18	16943.41	204.97	< LOD	74.54	14189.10	238.45
175FU32	5124.58	246.36	7645.39	123.91	< LOD	58.51	21522.52	268.27
175FU33	2790.33	224.00	4896.50	103.57	< LOD	59.21	22662.05	272.08
175FU34	2577.37	234.25	4941.38	108.85	< LOD	63.97	25242.25	298.09
175FU35	2387.71	232.84	5328.36	111.86	< LOD	63.30	27671.46	308.62
175FU36	2671.59	226.43	4399.49	101.48	< LOD	62.14	26909.48	310.35
175FU37	1996.23	230.34	7316.22	130.76	< LOD	64.65	26668.39	305.79
175FU38	2171.20	214.22	5601.24	111.26	< LOD	60.14	23399.14	280.73
175FU39	2014.96	229.73	8404.22	139.48	< LOD	65.04	24496.21	290.65
175FU40	2034.61	213.46	4425.54	100.46	< LOD	59.82	18414.49	228.62
175FU41	2639.33	217.44	3846.08	94.96	< LOD	60.09	16658.09	211.33

SAMPLE	Ca	Ca Error	Sc	Sc Error	Ba	Ba Error
175HC1	2073.27	52.91	16.16	11.95	< LOD	32.39
175HC2	6047.75	75.24	22.76	16.81	< LOD	28.56
175HC3	16940.19	267.77	93.02	26.33	< LOD	19.52
175FU1	12626.64	243.97	114.61	33.42	< LOD	18.65
175FU2	9027.38	134.86	40.84	22.25	< LOD	23.41
175FU3	7823.79	100.03	39.37	16.53	< LOD	19.19
175FU4	1989.66	60.08	< LOD	13.87	< LOD	29.09
175FU5	1678.56	56.74	< LOD	13.10	< LOD	30.07
175FU6	2100.67	61.19	< LOD	15.68	< LOD	37.18
175FU7	1514.16	56.68	< LOD	13.23	< LOD	30.63
175FU8	807.80	47.71	< LOD	10.83	< LOD	32.54
175FU9	1092.90	52.95	< LOD	12.34	< LOD	32.15
175FU10	1043.84	51.69	< LOD	12.18	< LOD	32.16
175FU11	1446.03	65.85	< LOD	16.06	< LOD	34.09
175FU12	1109.58	56.92	< LOD	13.55	< LOD	33.92
175FU13	3233.76	75.96	23.24	15.28	< LOD	32.61
175FU14	1267.79	57.55	< LOD	13.79	< LOD	31.61
175FU15	2375.99	70.63	18.38	16.23	972.53	26.77
175FU16	1001.44	55.35	< LOD	13.67	< LOD	33.13
175FU17	496.10	28.94	< LOD	8.11	< LOD	28.78
175FU18	7137.03	105.62	30.96	18.91	< LOD	35.42
175FU19	620.65	38.61	< LOD	14.54	< LOD	30.60
175FU20	596.28	29.81	9.47	8.58	< LOD	28.53
175FU21	2579.87	63.41	21.92	14.15	< LOD	32.25
175FU22	2394.08	64.13	24.65	14.25	< LOD	24.25
175FU23	4519.82	100.35	40.28	17.78	< LOD	22.38
175FU24	3184.40	76.90	26.82	15.08	< LOD	26.65
175FU25	2789.16	66.92	23.15	13.24	< LOD	30.68
175FU26	679.33	38.51	< LOD	9.03	< LOD	31.02
175FU27	541.29	36.31	< LOD	8.38	< LOD	33.03
175FU28	461.59	35.87	< LOD	8.29	< LOD	31.95
175FU29	533.39	35.15	< LOD	7.99	< LOD	32.49
175FU30	1005.09	41.05	< LOD	9.88	412.30	22.59
175FU31	5722.48	78.89	28.30	15.52	< LOD	31.81
175FU32	3254.48	71.41	< LOD	15.98	< LOD	33.74
175FU33	18576.02	317.77	60.86	22.61	< LOD	36.65
175FU34	22133.52	359.77	65.31	24.59	< LOD	35.93
175FU35	20749.39	348.17	70.83	23.96	< LOD	38.06
175FU36	19570.95	348.26	61.13	23.92	177.89	34.87
175FU37	23750.38	373.21	82.68	26.11	304.30	24.34
175FU38	23771.60	362.59	66.88	25.78	171.27	23.89
175FU39	28675.41	399.31	74.45	27.60	< LOD	36.86
175FU40	39497.34	417.49	66.37	37.37	217.12	24.03
175FU41	40820.19	412.45	51.93	30.00	230.44	23.37

Appendix Table 2. All detected values measured at Mud Buttes section in this study. Elements below the detection limit (<LOD) ranges between 0 and the displayed error. All values given in ppm.

SAMPLE	Ti	Ti Error	V	V Error	Cr	Cr Error	Mn	Mn Error
177HC4	4476.75	66.69	149.28	19.27	194.78	17.77	< LOD	40.05
177HC3	4597.91	68.71	167.46	20.03	215.86	24.35	< LOD	37.76
177HC2	4658.02	69.80	191.97	20.56	217.83	26.96	< LOD	37.03
177HC1	4021.34	65.49	157.48	19.48	184.93	17.23	< LOD	35.91
177FU2	11200.91	127.23	174.36	42.68	< LOD	18.61	< LOD	45.80
177FU3	8053.99	88.16	191.94	24.34	< LOD	16.58	< LOD	34.41
177FU4	10989.58	110.44	463.84	31.73	275.68	26.15	< LOD	30.87
177FU5	4478.77	54.46	91.05	15.41	< LOD	10.88	66.30	25.03
177FU6	4748.53	54.89	87.88	15.13	< LOD	11.03	< LOD	33.83
177FU7	4001.10	48.32	59.47	13.32	< LOD	10.19	< LOD	34.37
177FU8	4907.22	56.93	94.36	15.73	< LOD	11.48	< LOD	36.10
177FU11	3788.45	64.66	168.23	22.88	< LOD	15.15	< LOD	41.38
177FU13	4081.12	70.45	205.67	26.92	234.87	22.89	132.82	31.28
177FU14	4150.57	69.65	152.88	20.53	255.34	19.45	65.95	29.83

SAMPLE	Fe	Fe Error	Ni	Ni Error	Cu	Cu Error	Zn	Zn Error
177HC4	34015.91	230.08	53.14	19.28	64.48	8.96	61.94	5.86
177HC3	34518.22	228.58	72.25	20.81	73.62	9.03	70.25	5.99
177HC2	33280.51	220.78	49.80	18.58	71.77	8.85	45.72	5.63
177HC1	25436.77	190.08	49.69	18.51	51.16	8.30	32.75	4.70
177FU2	62253.33	334.04	< LOD	24.43	92.52	9.76	< LOD	5.96
177FU3	29105.12	200.80	40.43	19.49	171.99	10.71	23.92	4.51
177FU4	20370.20	158.88	129.50	18.25	64.55	8.12	33.16	4.32
177FU5	7279.54	86.50	< LOD	20.87	47.24	8.28	14.19	4.06
177FU6	11853.14	129.94	< LOD	20.50	51.32	8.30	23.95	4.32
177FU7	6185.18	74.05	< LOD	20.80	41.95	8.19	18.91	4.19
177FU8	14892.48	147.41	< LOD	21.19	56.70	8.56	27.58	4.60
177FU11	38471.21	249.60	78.43	22.70	99.65	9.88	84.26	6.60
177FU13	41559.27	261.45	73.05	19.74	81.52	9.49	98.28	7.65
177FU14	41913.08	264.31	67.40	22.96	92.25	9.77	104.34	7.66

SAMPLE	As	As Error	Se	Se Error	Rb	Rb Error	Sr	Sr Error
177HC4	46.99	6.18	< LOD	2.12	27.53	1.05	74.05	1.95
177HC3	32.97	6.04	< LOD	2.12	27.85	1.05	85.06	2.05
177HC2	23.20	5.14	< LOD	2.07	38.46	1.51	93.37	2.10
177HC1	27.30	5.03	< LOD	1.99	24.34	1.40	111.34	2.24
177FU2	301.74	10.37	< LOD	2.42	< LOD	1.40	88.33	2.20
177FU3	51.44	7.08	5.13	1.50	4.34	0.97	231.60	3.12
177FU4	78.05	6.53	5.46	1.41	7.55	1.13	414.36	3.91
177FU5	22.69	5.51	< LOD	2.14	34.51	1.61	101.84	2.18
177FU6	20.20	5.52	< LOD	2.09	36.89	1.64	86.17	2.00
177FU7	13.68	5.17	< LOD	2.11	31.57	1.56	75.62	1.91
177FU8	23.05	5.55	< LOD	2.14	23.73	1.00	93.79	2.12
177FU11	33.24	6.55	2.56	1.79	52.36	1.42	152.60	2.76
177FU13	15.21	6.12	< LOD	2.28	56.36	1.47	106.68	2.35
177FU14	17.93	6.14	< LOD	2.30	57.65	1.49	110.32	2.40

SAMPLE	Y	Y Error	Zr	Zr Error	Nb	Nb Error	Mo	Mo Error
177HC4	11.01	1.38	148.13	2.77	9.79	1.17	4.69	1.38
177HC3	15.24	1.43	172.04	2.91	11.28	1.18	5.61	1.31
177HC2	17.25	1.40	167.53	2.84	9.80	1.15	5.81	1.28
177HC1	12.31	1.26	157.13	2.74	6.02	1.08	4.55	1.25
177FU2	2.51	1.46	58.50	2.12	6.48	1.15	10.59	1.52
177FU3	20.43	1.33	245.06	3.34	6.15	1.10	14.80	1.39
177FU4	51.42	1.68	526.79	4.47	5.39	1.13	27.06	1.57
177FU5	30.30	1.60	600.11	4.94	12.78	1.21	10.00	1.54
177FU6	29.48	1.57	466.12	4.35	12.70	1.20	6.66	1.43
177FU7	23.70	1.51	542.12	4.71	10.34	1.17	6.83	1.49
177FU8	28.49	1.61	652.40	5.18	13.46	1.23	9.59	1.58
177FU11	27.64	1.78	205.96	3.30	12.79	1.28	9.92	1.42
177FU13	18.02	1.68	133.93	2.76	10.58	1.23	3.18	1.30
177FU14	22.01	1.75	149.57	2.91	12.50	1.27	4.53	1.34

SAMPLE	W	W Error	Hg	Hg Error	Pb	Pb Error	Bi	Bi Error
177HC4	80.87	20.77	< LOD	6.04	12.54	2.54	< LOD	9.48
177HC3	< LOD	16.93	< LOD	5.91	17.55	2.73	< LOD	9.55
177HC2	71.05	18.08	< LOD	5.80	10.01	2.35	< LOD	9.37
177HC1	< LOD	15.78	< LOD	5.55	7.83	2.19	< LOD	9.01
177FU2	91.68	19.53	< LOD	6.42	35.04	3.54	< LOD	9.37
177FU3	< LOD	15.46	8.29	3.81	32.72	3.18	< LOD	9.79
177FU4	< LOD	14.51	6.04	4.27	17.82	2.55	< LOD	10.46
177FU5	89.94	21.90	6.35	5.42	14.91	2.55	< LOD	10.34
177FU6	< LOD	15.89	< LOD	5.68	16.29	2.62	< LOD	9.92
177FU7	52.61	19.82	< LOD	5.73	12.60	2.49	< LOD	10.01
177FU8	104.86	22.19	< LOD	5.91	14.33	2.60	< LOD	10.70
177FU11	139.55	24.23	7.38	5.96	21.97	3.06	< LOD	10.77
177FU13	99.13	19.87	< LOD	6.25	22.57	3.07	< LOD	10.18
177FU14	98.05	22.14	< LOD	6.39	21.84	3.06	< LOD	10.45

SAMPLE	Th	Th Error	U	U Error	Mg	Mg Error	Al	Al Error
177HC4	7.20	1.86	5.08	3.07	10849.22	3320.82	59411.22	1386.45
177HC3	8.67	2.38	5.65	2.74	14240.91	3648.46	66620.97	1557.64
177HC2	6.94	1.77	4.70	2.56	12543.16	3525.60	67470.62	1538.41
177HC1	4.72	2.12	5.66	2.35	10141.93	2994.04	72765.39	1460.91
177FU2	6.71	4.14	8.74	2.31	16265.04	3797.33	80443.74	1805.90
177FU3	16.24	4.09	11.39	2.33	8693.52	3299.70	66915.47	1531.37
177FU4	14.74	3.02	28.18	2.77	6751.33	3099.18	19855.11	856.34
177FU5	9.96	1.83	7.35	2.57	< LOD	5568.56	42796.10	1239.29
177FU6	9.22	1.79	8.20	2.58	7210.97	5392.73	49311.96	1351.48
177FU7	8.40	1.76	6.69	2.49	8400.71	3760.81	46202.64	1209.17
177FU8	10.41	1.89	8.30	2.69	< LOD	6457.08	50521.59	1412.88
177FU11	11.53	2.15	3.81	1.06	14503.14	4436.63	66875.90	1781.06
177FU13	10.47	2.14	2.80	1.64	14792.11	4087.31	70356.16	1722.01
177FU14	10.73	2.17	2.74	1.03	18105.80	4377.15	70369.47	1788.89

SAMPLE	Si	Si Error	P	P Error	S	S Error	Cl	Cl Error
177HC4	260570.1	1331.09	2719.40	187.27	3019.61	74.11	< LOD	49.96
177HC3	283758.3	1380.08	4281.54	212.28	3083.27	77.60	< LOD	52.98
177HC2	265849.0	1336.25	3527.49	199.72	5209.53	95.96	< LOD	51.37
177HC1	218152.4	1207.76	3326.66	172.55	5891.00	95.07	< LOD	47.10
177FU2	215197.6	1280.77	1533.15	174.63	3632.29	84.15	< LOD	54.51
177FU3	187035.3	1196.08	2037.14	175.30	11277.37	142.85	< LOD	54.46
177FU4	71689.55	792.54	1204.95	147.02	26407.75	221.03	93.99	34.89
177FU5	357639.8	1628.07	68454.53	2056.40	5790.98	145.71	< LOD	53.99
177FU6	349804.0	1475.73	8699.59	255.88	2180.05	67.62	< LOD	51.71
177FU7	354358.2	1482.89	7153.17	241.05	1904.86	62.20	< LOD	49.61
177FU8	348443.8	1623.59	45317.72	2031.00	5040.14	142.37	< LOD	55.88
177FU11	298394.4	1469.86	3209.74	235.48	6510.90	120.08	< LOD	63.19
177FU13	275474.2	1398.78	3267.89	213.54	2727.95	78.58	< LOD	57.51
177FU14	286116.1	1434.04	3240.93	222.28	2227.23	75.14	< LOD	60.32

SAMPLE	K	K Error	Ca	Ca Error	Sc	Sc Error	Ba	Ba Error
177HC4	8209.34	154.36	1216.64	52.37	14.50	11.93	< LOD	37.60
177HC3	7960.09	153.69	1603.06	57.19	< LOD	14.16	< LOD	34.86
177HC2	6822.59	145.64	2454.45	66.11	< LOD	16.32	< LOD	33.22
177HC1	5135.10	130.26	3034.78	66.68	18.17	13.98	< LOD	33.40
177FU2	967.07	83.36	2020.88	68.54	22.01	18.27	< LOD	38.29
177FU3	2345.25	97.59	6311.04	94.19	35.85	17.85	< LOD	28.96
177FU4	3001.68	104.31	16257.84	288.86	105.11	29.79	< LOD	22.51
177FU5	11108.22	166.27	1375.27	41.55	< LOD	9.98	429.57	22.66
177FU6	11365.59	172.65	1251.35	42.63	< LOD	9.98	< LOD	33.31
177FU7	10912.74	159.85	958.86	37.26	< LOD	8.65	< LOD	34.86
177FU8	12038.40	186.43	1382.84	44.63	< LOD	10.43	< LOD	33.13
177FU11	20640.13	298.08	4016.64	84.85	26.77	16.36	< LOD	32.41
177FU13	21223.27	297.60	3362.81	85.09	< LOD	19.23	235.16	35.20
177FU14	22404.09	309.92	3832.33	87.23	21.38	16.57	< LOD	37.19

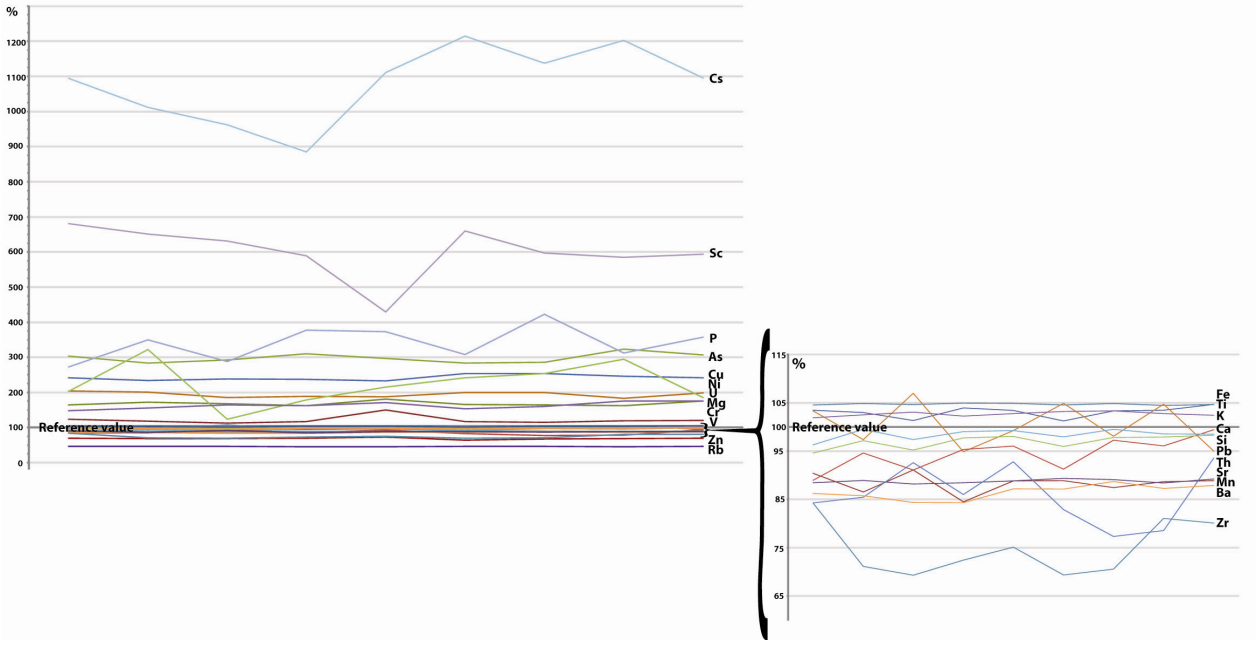

Appendix Fig. 5. Plot of calibration values measured on standard sample 2709a every tenth sample. 100% represents the standards reference value. Elements closest to the reference value (100% correct) is enlarged on the right side to display their distribution. All values given in ppm.

Appendix Table 3. Analyses of standard sample 2709a measured every tenth sample. The standards known elements concentration , reference value, is displayed in the bottom row below each element. All values given in ppm.

STANDARD	Ti	Ti Error	V	V Error	Cr	Cr Error	Mn	Mn Error
2709a	3476.16	68.01	135.84	20.45	214.03	28.65	478.21	41.37
2709a	3459.62	67.69	129.53	20.21	223.26	28.79	457.72	41.06
2709a	3404.91	68.12	124.24	20.34	218.47	29.27	481.91	41.62
2709a	3491.80	68.85	128.13	20.54	211.23	29.23	446.95	40.86
2709a	3475.46	68.59	165.56	26.12	235.91	28.75	470.00	41.29
2709a	3402.55	68.17	128.35	20.42	215.06	29.05	470.19	41.55
2709a	3471.26	68.62	126.23	20.43	213.09	29.18	462.67	41.26
2709a	3476.56	68.33	130.97	20.47	210.78	28.87	468.93	41.43
2709a	3516.99	68.24	132.37	20.36	227.72	28.76	470.19	41.47
Average	**3463.92**	**68.29**	**133.47**	**21.04**	**218.84**	**28.95**	**467.42**	**41.32**
Reference	**3360**	**70**	**110**	**11**	**130**	**9**	**529**	**18**

STANDARD	Fe	Fe Error	Co	Co Error	Ni	Ni Error	Cu	Cu Error
2709a	35127.84	255.29	< LOD	68.24	173.50	22.89	81.75	10.30
2709a	35225.92	256.43	< LOD	68.16	170.64	22.86	79.16	10.26
2709a	35163.46	256.79	< LOD	68.54	157.72	22.74	80.99	10.31
2709a	35258.92	256.68	< LOD	68.54	160.38	22.74	80.62	10.29
2709a	35242.14	256.36	< LOD	68.39	159.21	22.69	78.92	10.23
2709a	35128.78	257.38	< LOD	68.86	169.99	23.02	85.87	10.47
2709a	35231.28	257.10	< LOD	68.42	170.12	22.93	86.10	10.46
2709a	35099.38	256.66	< LOD	68.58	155.62	22.87	83.60	10.40
2709a	35160.54	256.77	< LOD	68.57	169.09	22.94	81.81	10.35
Average	**35182.03**	**256.61**	**< LOD**	**68.48**	**165.14**	**22.85**	**82.09**	**10.34**
Reference	**33600**	**700**	**12.8**	**0.2**	**85**	**2**	**33.9**	**0.5**

STANDARD	Zn	Zn Error	As	As Error	Rb	Rb Error	Sr	Sr Error
2709a	72.17	6.72	31.84	6.70	45.84	1.43	211.37	3.45
2709a	70.71	6.70	29.73	6.64	45.89	1.44	212.54	3.47
2709a	70.91	6.74	30.73	6.76	45.70	1.44	210.77	3.47
2709a	71.20	6.72	32.61	6.62	45.18	1.43	211.42	3.46
2709a	75.08	6.83	31.21	6.69	45.25	1.43	212.37	3.47
2709a	66.01	6.63	29.79	6.68	45.62	1.44	213.58	3.49
2709a	69.30	6.70	29.98	6.64	46.12	1.44	212.92	3.48
2709a	70.06	6.73	33.98	6.76	45.16	1.43	211.26	3.47
2709a	71.37	6.75	32.19	6.64	45.86	1.45	213.23	3.49
Average	**70.75**	**6.72**	**31.34**	**6.68**	**45.62**	**1.44**	**212.16**	**3.47**
Reference	**103**	**4**	**10.5**	**0.3**	**99**	**3**	**239**	**6**

STANDARD	Zr	Zr Error	Cd	Cd Error	Sb	Sb Error	Hg	Hg Error
2709a	164.29	3.30	< LOD	9.24	< LOD	15.65	< LOD	6.96
2709a	138.74	3.12	< LOD	9.19	< LOD	15.72	< LOD	7.11
2709a	135.11	3.10	< LOD	9.18	< LOD	15.63	< LOD	7.13
2709a	141.24	3.14	< LOD	9.18	< LOD	15.52	< LOD	7.04
2709a	146.53	3.18	< LOD	9.18	< LOD	15.57	< LOD	7.03
2709a	135.22	3.11	< LOD	9.31	< LOD	15.71	< LOD	7.10
2709a	137.63	3.12	< LOD	9.25	< LOD	15.74	< LOD	7.12
2709a	158.12	3.28	< LOD	9.24	< LOD	15.67	< LOD	7.15
2709a	156.24	3.27	< LOD	9.26	< LOD	15.71	< LOD	7.12
Average	**145.90**	**3.18**	**< LOD**	**9.23**	**< LOD**	**15.66**	**< LOD**	**7.08**
Reference	**195**	**46**	**0.371**	**0.002**	**1.55**	**0.06**	**0.9**	**0.2**

STANDARD	Pb	Pb Error	Th	Th Error	U	U Error	Mg	Mg Error
2709a	17.88	3.08	9.19	2.19	6.39	3.56	21668.49	4722.38
2709a	16.85	3.05	9.32	2.20	10.15	3.67	22730.07	4828.45
2709a	18.51	3.14	10.10	2.23	3.88	1.94	23990.80	4786.56
2709a	16.41	3.04	9.38	2.20	5.65	2.38	23741.82	4898.53
2709a	17.17	3.06	10.11	2.23	6.77	2.99	25009.60	4931.93
2709a	18.15	3.12	9.04	2.20	7.61	3.63	22326.60	4768.12
2709a	16.97	3.05	8.43	2.17	8.00	3.64	23362.76	4866.91
2709a	18.11	3.11	8.56	2.18	9.28	3.65	25599.85	4958.07
2709a	16.43	3.05	10.20	2.24	5.84	2.41	25654.49	4953.45
Average	**17.39**	**3.08**	**9.37**	**2.20**	**7.06**	**3.10**	**23787.16**	**4857.15**
Reference	**17.3**	**0.1**	**10.9**	**0.2**	**3.15**	**0.05**	**14600**	**200**

STANDARD	Al	Al Error	Si	Si Error	P	P Error	K	K Error
2709a	65565.38	1805.79	286624.0	1491.53	1878.83	218.78	21504.61	291.28
2709a	69723.32	1890.07	294358.4	1504.52	2409.81	226.20	21625.50	292.30
2709a	67147.04	1834.43	288515.6	1494.37	1979.91	219.11	21744.17	295.29
2709a	70268.62	1919.67	296095.8	1518.41	2598.80	229.98	21570.67	293.45
2709a	70785.53	1928.17	296994.0	1514.74	2568.07	229.33	21688.52	293.90
2709a	67271.26	1838.97	290710.5	1502.73	2116.16	222.26	21774.98	294.90
2709a	71668.94	1929.99	296406.3	1511.10	2909.80	229.97	21798.71	294.55
2709a	70811.63	1936.07	296669.1	1517.48	2149.72	228.49	21688.08	294.02
2709a	73283.42	1985.02	297869.3	1518.00	2456.57	228.94	21611.01	292.70
Average	**69613.90**	**1896.46**	**293804.8**	**1508.10**	**2340.85**	**225.90**	**21667.36**	**293.60**
Reference	**73700**	**1600**	**303000**	**4000**	**688**	**13**	**21100**	**600**

STANDARD	Ca	Ca Error	Sc	Sc Error	Cs	Cs Error	Ba	Ba Error
2709a	18395.86	351.26	75.58	26.29	54.72	14.93	844.21	30.68
2709a	19009.35	353.75	72.28	26.39	50.61	14.91	839.43	30.65
2709a	18600.98	355.86	70.01	26.36	48.13	14.90	826.15	30.59
2709a	18918.47	355.18	65.42	26.59	44.23	14.77	825.51	30.38
2709a	18957.81	355.24	47.67	26.41	55.58	14.86	853.52	30.56
2709a	18711.13	354.58	73.25	26.30	60.74	15.00	853.15	30.81
2709a	19008.66	354.78	66.30	26.62	56.89	14.97	868.24	30.83
2709a	18823.16	354.64	64.91	26.45	60.15	14.93	854.34	30.67
2709a	18819.11	353.12	65.94	26.34	54.78	14.94	860.16	30.77
Average	**18804.95**	**354.27**	**66.82**	**26.42**	**53.98**	**14.91**	**847.19**	**30.66**
Reference	**19100**	**900**	**11.1**	**0.1**	**5**	**0.1**	**979**	**28**

STANDARD	La	La Error	Ce	Ce Error
2709a	< LOD	1.5	< LOD	1.5
2709a	< LOD	1.5	< LOD	1.5
2709a	< LOD	1.5	< LOD	1.5
2709a	< LOD	1.5	< LOD	1.5
2709a	< LOD	1.5	< LOD	1.5
2709a	< LOD	1.5	< LOD	1.5
2709a	< LOD	1.5	< LOD	1.5
2709a	< LOD	1.5	< LOD	1.5
2709a	< LOD	1.5	< LOD	1.5
Average	**< LOD**	**1.5**	**< LOD**	**1.5**
Reference	**21.7**	**0.4**	**42**	**1**

Tidigare skrifter i serien "Examensarbeten i Geologi vid Lunds universitet":

306. Lundberg, Frans, 2012: Den senkambriska alunskiffern i Västergötland – utbredning, mäktigheter och faciestyper. (15 hp)
307. Thulin Olander, Henric, 2012: Hydrogeologisk kartering av grundvattenmagasinet Ekenäs-Kvarndammen, Jönköpings län. (15 hp)
308. Demirer, Kursad, 2012: U-Pb baddeleyite ages from mafic dyke swarms in Dharwar craton, India – links to an ancient supercontinent. (45 hp)
309. Leskelä, Jari, 2012: Loggning och återfyllning av borrhål – Praktiska försök och utveckling av täthetskontroll i fält. (15 hp)
310. Eriksson, Magnus, 2012: Stratigraphy, facies and depositional history of the Colonus Shale Trough, Skåne, southern Sweden. (45 hp)
311. Larsson, Amie, 2012: Kartläggning, beskrivning och analys av Kalmar läns regionalt viktiga vattenresurser. (15 hp)
312. Olsson, Håkan, 2012: Prediction of the degree of thermal breakdown of limestone: A case study of the Upper Ordovician Boda Limestone, Siljan district, central Sweden. (45 hp)
313. Kampmann, Tobias Christoph, 2012: U-Pb geochronology and paleomagnetism of the Westerberg sill, Kaapvaal Craton – support for a coherent Kaapvaal-Pilbara block (Vaalbara). (45 hp)
314. Eliasson, Isabelle Timms, 2012: Arsenik: förekomst, miljö och hälsoeffekter. (15 hp)
315. Badawy, Ahmed Salah, 2012: Sequence stratigraphy, palynology and biostratigraphy across the Ordovician-Silurian boundary in the Röstånga-1 core, southern Sweden. (45 hp)
316. Knut, Anna, 2012: Resistivitets- och IP-mätningar på Flishultsdeponin för lokalisering av grundvattenytor. (15 hp)
317. Nylén, Fredrik, 2012: Förädling av ballastmaterial med hydrocyklon, ett fungerande alternativ? (15 hp)
318. Younes, Hani, 2012: Carbon isotope chemostratigraphy of the Late Silurian Lau Event, Gotland, Sweden. (45 hp)
319. Weibull, David, 2012: Subsurface geological setting in the Skagerrak area – suitability for storage of carbon dioxide. (15 hp)
320. Petersson, Albin, 2012: Förutsättningar för geoenergi till idrottsanläggningar i Kallerstad, Linköpings kommun: En förstudie. (15 hp)
321. Axbom, Jonna, 2012: Klimatets och människans inverkan på tallens etablering på sydsvenska mossar under de senaste århundradena – en dendrokronologisk och torvstratigrafisk analys av tre småländska mossar. (15 hp)
322. Kumar, Pardeep, 2012: Palynological investigation of coal-bearing deposits of the Thar Coal Field Sindh, Pakistan. (45 hp)
323. Gabrielsson, Johan, 2012: Havsisen i arktiska bassängen – nutid och framtid i ett globalt uppvärmningsperspektiv. (15 hp)
324. Lundgren, Linda, 2012: Variation in rock quality between metamorphic domains in the lower levels of the Eastern Segment, Sveconorwegian Province. (45 hp)
325. Härling, Jesper, 2012: The fossil wonders of the Silurian Eramosa Lagerstätte of Canada: the jawed polychaete faunas. (15 hp)
326. Qvarnström, Martin, 2012: An interpretation of oncoid mass-occurrence during the Late Silurian Lau Event, Gotland, Sweden. (15 hp)
327. Ulmius, Jan, 2013: P-T evolution of paragneisses and amphibolites from Romeleåsen, Scania, southernmost Sweden. (45 hp)
328. Hultin Eriksson, Elin, 2013: Resistivitetsmätningar för avgränsning av lakvattenplym från Kejsarkullens deponis infiltrationsområde. (15 hp)
329. Mozafari Amiri, Nasim, 2013: Field relations, petrography and 40Ar/39Ar cooling ages of hornblende in a part of the eclogite-bearing domain, Sveconorwegian Orogen. (45 hp)
330. Saeed, Muhammad, 2013: Sedimentology and palynofacies analysis of Jurassic rocks Eriksdal, Skåne, Sweden. (45 hp)
331. Khan, Mansoor, 2013: Relation between sediment flux variation and land use patterns along the Swedish Baltic Sea coast. (45 hp)
332. Bernhardson, Martin, 2013: Ice advance-retreat sediment successions along the Logata River, Taymyr Peninsula, Arctic Siberia. (45 hp)
333. Shrestha, Rajendra, 2013: Optically Stimulated Luminescence (OSL) dating

of aeolian sediments of Skåne, south Sweden. (45 hp)

334. Fullerton, Wayne, 2013: The Kalgoorlie Gold: A review of factors of formation for a giant gold deposit. (15 hp)
335. Hansson, Anton, 2013: A dendroclimatic study at Store Mosse, South Sweden – climatic and hydrologic impacts on recent Scots Pine (*Pinus sylvestris*) growth dynamics. (45 hp)
336. Nilsson, Lawrence, 2013: The alteration mineralogy of Svartliden, Sweden. (30 hp)
337. Bou-Rabee, Donna, 2013: Investigations of a stalactite from Al Hota cave in Oman and its implications for palaeoclimatic reconstructions. (45 hp)
338. Florén, Sara, 2013: Geologisk guide till Söderåsen – 17 geologiskt intressanta platser att besöka. (15 hp)
339. Kullberg, Sara, 2013: Asbestkontamination av dricksvatten och associerade risker. (15 hp)
340. Kihlén, Robin, 2013: Geofysiska resistivitetsmätingar i Sjöcrona Park, Helsingborg, undersökning av områdets geologiska egenskaper samt 3D modellering i GeoScene3D. (15 hp)
341. Linders, Wictor, 2013: Geofysiska IP-undersökningar och 3D-modellering av geofysiska samt geotekniska resultat i GeoScene3D, Sjöcrona Park, Helsingborg, Sverige. (15 hp)
342. Sidenmark, Jessica, 2013: A reconnaissance study of Rävliden VHMS-deposit, northern Sweden. (15 hp)
343. Adamsson, Linda, 2013: Peat stratigraphical study of hydrological conditions at Stass Mosse, southern Sweden, and the relation to Holocene bog-pine growth. (45 hp)
344. Gunterberg, Linnéa, 2013: Oil occurrences in crystalline basement rocks, southern Norway – comparison with deeply weathered basement rocks in southern Sweden. (15 hp)
345. Peterffy, Olof, 2013: Evidence of epibenthic microbial mats in Early Jurassic (Sinemurian) tidal deposits, Kulla Gunnarstorp, southern Sweden. (15 hp)
346. Sigeman, Hanna, 2013: Early life and its implications for astrobiology – a case study from Bitter Springs Chert, Australia. (15 hp)
347. Glommé, Alexandra, 2013: Texturella studier och analyser av baddeleyitomvandlingar i zirkon, exempel från sydöstra Ghana. (15 hp)
348. Brådenmark, Niklas, 2013: Alunskiffer på Öland – stratigrafi, utbredning, mäktigheter samt kemiska och fysikaliska egenskaper. (15 hp)
349. Jalnefur Andersson, Evelina, 2013: En MIFO fas 1-inventering av fyra potentiellt förorenade områden i Jönköpings län. (15 hp)
350. Eklöv Pettersson, Anna, 2013: Monazit i Obbhult-komplexet: en pilotstudie. (15 hp)
351. Acevedo Suez, Fernando, 2013: The reliability of the first generation infrared refractometers. (15 hp)
352. Murase, Takemi, 2013: Närkes alunskiffer – utbredning, beskaffenhet och oljeinnehåll. (15 hp)
353. Sjöstedt, Tony, 2013: Geoenergi – utvärdering baserad på ekonomiska och drifttekniska resultat av ett passivt geoenergisystem med värmeuttag ur berg i bostadsrättsföreningen Mandolinen i Lund. (15 hp)
354. Sigfúsdóttir, Thorbjörg, 2013: A sedimentological and stratigraphical study of Veiki moraine in northernmost Sweden. (45 hp)
355. Månsson, Anna, 2013: Hydrogeologisk kartering av Hultan, Sjöbo kommun. (15 hp)
356. Larsson, Emilie, 2013: Identifying the Cretaceous–Paleogene boundary in North Dakota, USA, using portable XRF. (15 hp)

LUNDS UNIVERSITET

Geologiska institutionen
Lunds universitet
Sölvegatan 12, 223 62 Lund